

# **Fuel-Flexible Combustion System for Co-production Plant Applications**

## **Semi-Annual Report**

**January 2006**

**June 2006**

**Joel Haynes, Craig Russell, Matt Mosbacher,  
Tim Lieuwen, Suresh Menon, Jerry Seitzman**

**July 2006**

**DE-FC26-03NT41776**

**GE Global Research  
1 Research Circle  
Niskayuna, NY 12309**

## ***DISCLAIMER***

This report was prepared as an account of work sponsored by an agency of the United States Government. Neither the United States Government nor any agency thereof, nor any of their employees, makes any warranty, express or implied, or assumes any legal liability or responsibility for the accuracy, completeness, or usefulness of any information, apparatus, product, or process disclosed, or represents that its use would not infringe privately owned rights. Reference herein to any specific commercial product, process, or service by trade name, trademark, manufacturer, or otherwise does not necessarily constitute or imply its endorsement, recommendation, or favoring by the United States Government or any agency thereof. The views and opinions of authors expressed herein do not necessarily state or reflect those of the United States Government or any agency thereof.

## **Abstract**

Future high-efficiency, low-emissions generation plants that produce electric power, transportation fuels, and/or chemicals from fossil fuel feed stocks require a new class of fuel-flexible combustors. In this 36-month program, a validated combustor approach will be developed which will enable single-digit  $\text{NO}_x$  operation of future generation plants with low-Btu off gas and high-hydrogen fuels, with the flexibility of process-independent backup with both natural gas and liquid fuels. This combustion technology will overcome the limitations of current syngas gas turbine combustion systems, which are designed on a site-by-site basis, and enable improved future co-generation plant designs. In this capacity, a fuel-flexible combustor will enhance the efficiency and productivity of future co-production plants.

This report discusses the development and design of a syngas capable TVC combustor. The TVC combustor premixes the syngas with air for low emission performance. The combustor was designed for operation with syngas and no additional diluents. The combustor was successfully operated at targeted gas turbine conditions. Four kinetic mechanisms for syngas has also been evaluated. The first is mechanism is GRI Mech 3.0, a well-tested mechanism that has been validated extensively for methane chemistry, and therefore also includes oxy-hydrogen and carbon monoxide mechanisms. The second mechanism is a mechanism developed recently for  $\text{H}_2/\text{CO}$  combustion. The other two mechanism were developed for this program by J. Y. Chen. They are reduced mechanism: one uses 14 species, the other tracks only 9 species. This reduced mechanism has been applied to an LES model of the hybrid prototype which was discussed in the previous report.

## Table of Contents

DISCLAIMER .....	2
Abstract .....	3
Table of Contents .....	4
List of Graphics .....	5
1 Introduction .....	7
1.2 Task 2 (Fuel Flexible Combustor Design Approaches) .....	7
1.3 Task 3 (Syngas Flame characterization).....	7
1.4 Task 4 (Systems Plant Performance Modeling) .....	9
1.5 Task 5 (Fuel Flexible Combustor Prototype Design).....	9
1.6 Task 6 (Syngas Methodology for Advanced CFD tools) .....	9
Executive Summary .....	11
2 Experimental .....	13
2.1 Task 3 (Syngas Fuel Flame Characterization).....	13
2.1.1 Apparatus .....	13
2.1.2 Experimental and operating data .....	14
2.1.3 Data Reduction.....	16
2.2 Task 5 (Prototype Design).....	16
2.2.1 Trapped Vortex Combustor Design (Prototype-2) .....	16
2.2.2 Instrumentation.....	19
2.3 Task 6 (Advanced CFD tools).....	21
2.3.1 Apparatus .....	21
2.3.1.1 Syngas Methodology for Advanced CFD tools.....	21
2.3.1.2 LES Mathematical Formulation .....	22
2.3.1.3 LES Subgrid Closure Methods.....	23
3 Results and Discussion.....	24
3.1 Task 3 (Syngas Fuel Flame Characterization).....	24
3.1.1 Model Comparisons: Effect of Preheating and CO <sub>2</sub> Dilution .....	24
3.1.1.1 Effect of Preheat: Strained Laminar Flame Speed Measurement.....	24
3.1.1.2 Effect of Preheat and Dilution: Strained Laminar Flame Speed Measurement	26
3.2 Task 5 (Prototype Design).....	27
3.2.1 Trapped Vortex Combustor (Prototype-2) Experimental Results .....	27
3.3 Task 6 (Syngas Methodology for Advanced CFD Tools) .....	31
3.3.1 Chemical Mechanism Validation .....	31
3.3.2 LES Computations .....	32
4 Conclusions .....	38
4.1 Task 3 (Syngas fuel flame characterization) .....	38
4.2 Task 5 (Prototype Design).....	38
4.3 Task 6 (Syngas Methodology for Advanced CFD Tools) .....	38
5 References .....	39

## List of Graphics

Figure 2.1-1: Schematic of stagnation flame burner. ....	14
Figure 2.1-2: Image of flame emission from a stagnation flame at $p=5.0$ atm for a fuel mixture $H_2:CO=10:90$ at an equivalence ratio $\phi=0.6$ ; average inflow velocity $\sim 4S_L$ ; $L/D=0.5$ . ....	15
Figure 2.1-3: Velocity measurements along the centerline of a stagnation flame for 90% CO and 10% $H_2$ fuel mixture, $\phi=0.6$ , $p=5.0$ atm at seven flow rates. The flow direction is right to left in this figure, i.e., cold reactants are present at 3.75 mm, while there are hot products at 1.5 mm. ....	15
Figure 2.1-4: Measured flame speeds corresponding to results shown in Figure 2.1-3. ....	16
Figure 2.2-1: Prototype-2 TVC Combustor Design Features. ....	18
Figure 2.2-2: Prototype-2 Air Flow Passages ....	18
Figure 2.2-3: Prototype-2 Thermocouple Locations ....	19
Figure 2.2-4: Prototype-2 pressure instrumentation nomenclature and locations ....	20
Figure 2.2-5: Prototype-2 Hardware ....	20
Figure 2.2-6: Prototype-2 water-cooled, hydrogen spark igniter located through impingement cooling sleeve and aft wall of the combustion cavity section ....	21
Figure 3.1-1 Flame speeds for a 50:50 $H_2:CO$ composition at 600 K preheat temperature for 0.6 equivalence ratios. (vertical bars on measurements indicate a 10% deviation band - not uncertainties in the measurements.) ....	25
Figure 3.1-2 Flame speeds for a 50:50 $H_2:CO$ composition at 700 K preheat temperature for two equivalence ratios. (vertical bar on measurements indicate 10% deviation from the data. It is not the error in measurement). ....	26
Figure 3.1-3: Flame speeds for a 30:30:40 $H_2:CO:CO_2$ composition at 700 K preheat temperature for two equivalence ratios. (vertical bar on measurements indicate 10% deviation from the data. It is not the error in measurement). ....	27
Figure 3.2-1: TVC Surface Temperatures with Syngas Combustion ....	29
Figure 3.2-2: TVC Dynamics Measurements with Syngas ....	29
Figure 3.2-3: TVC Exhaust Oxygen and $CO_2$ Concentrations with Syngas ....	30
Figure 3.2-4: TVC $NO_x$ Emission with Syngas ....	30
Figure 3.3-1: OH reaction rate contour plot superimposed onto vorticity surface plot for 5 step reduced mechanism at $t=$ a) 0.000512, b) 0.00102 sec and for 10 step reduced mechanism at $t=$ c) 0.000512, d) 0.00102 sec ....	32
Figure 3.3-2: a) Side view of the schematics of the combustor assembly, b) schematic view of the diffuser cap on the injection plane, and c) perspective view of the grid employed for the computations. ....	32
Figure 3.3-3 (a) perspective, (b) cross sectional, and (c) side view of the grid used for computations. Not all grid points are shown. ....	33
Figure 3.3-4 Spectra obtained from instantaneous U and V velocity data, probed at $(x,y) = (0.0211, 0.0402)$ m. ....	34
Figure 3.3-5 Time trace of (a) u velocity, (b) w velocity, and (c) v velocity at two different locations; and (d) location of the points where data are from. ....	34
Figure 3.3-6 Instantaneous surface plots of temperature superimposed onto velocity vectors: (a) side view; cross sections obtained at (b) $x=0.01239$ m, (c) 0.0182 m, (d) 0.0270 m away from the diffuser cap, and (e) close up side view along with $N_2$ mass fraction conto. ....	36

Figure 3.3-7(a) CO mass fraction surface plot with CO reaction rate contour plot obtained at  $x=0.01239$  m away from the diffuser cap. (b) Close up side view of CO mass fraction surface plot with vorticity contour plot. .... 36

Figure 3.3-8 Time averaged profiles of (a) u velocity and (b) temperature. .... 37

# 1 Introduction

## 1.2 Task 2 (Fuel Flexible Combustor Design Approaches)

The purpose of this task is to develop a technology scorecard to select two conceptual configurations for a low emissions fuel flexible combustor that burns natural gas and syngas fuels. This task was completed during the January-December 2004 reporting periods. Two combustor prototypes: a hybrid of a diffusion burner for syngas and premixed swirl burner for natural gas and a trapped vortex combustor for both syngas and natural gas were selected for further consideration. The methods and processes used in developing the technology scorecard along with preliminary modeling results from evaluating technologies for a fuel flexible combustor in Task 2 were presented in the previous reports. Details of the chemical kinetics calculations employed in Task 2 and the results thereof are presented in the January-May 2005 reporting period and published in the 2005 ASME Turbo-Expo (Iyer et al., 2005).

## 1.3 Task 3 (Syngas Flame characterization)

Combustor design tools for synthetic gas fuels will require simplified models for predicting combustor stability performance based on reduced order (e.g., time-averaged) quantities. Specifically, appropriate methodologies are needed to predict the effects of variable fuel composition upon combustor stability limits.

Our approach is to obtain experimental measurements of flame speed for ranges of synthetic gas compositions, and under ranges of temperature, pressure and strain. Laminar flame speed ( $S_L$ ) is defined as the velocity of steady, one-dimensional propagation of a planar, adiabatic, unstrained laminar flame into a uniform premixed fuel-air mixture at rest. Laminar flame speed is an important parameter, because it contains fundamental information regarding reactivity, diffusivity, and exothermicity of a combustible mixture.

In order to address the feasibility of synthetic gas for fuel-flexible gas turbine combustion, one must be able to accurately predict flame behavior under preheating and high-pressure conditions. Preheating increases reaction rates and diffusivity. Pressure not only influences molecular collision frequencies, but also the relative efficiencies of the two-body branching reactions versus the three-body termination reactions. Pressure changes the chemical kinetics and the flame speed; hence, data of  $S_L$  at high pressures is important and the experiments described below include plans for high pressure studies.

Syngas fuels also have a large variability in diluents content, e.g., the composition of  $\text{CO}_2$  can range from 1.6-30% (Zhu *et al.*, 1988). The presence of  $\text{CO}_2$  in the fuel will impact the flame in at least four ways, through changes in: 1) mixture specific heat, 2) adiabatic flame temperature, 3) chemical kinetic rates, and 4) radiative heat transfer. First, the molar specific heat of  $\text{CO}_2$  is larger than that for the fuels it displaces ( $\text{CO}$  and  $\text{H}_2$ ). Therefore the addition of  $\text{CO}_2$  will lower the reactant temperatures in the preheat region of the flame. Second, addition of any diluent reduces the adiabatic flame temperature, and thus the laminar flame speed. Since

CO<sub>2</sub> has a higher molar specific heat than air, it reduces the adiabatic flame temperature and flame speed more than an equal amount of air dilution. Thus the flammability limits and extinction strain rates of the CO<sub>2</sub> mixtures are correspondingly narrower.

Third, CO<sub>2</sub> does not act as a passive diluent in the fuel, but interacts kinetically. The kinetic effects of CO<sub>2</sub> dilution are manifested primarily in the main CO oxidation reaction,  $\text{CO} + \text{OH} \rightarrow \text{CO}_2 + \text{H}$ . Higher CO<sub>2</sub> levels lead to enhanced back reaction rates and, hence, reduced CO oxidation and enhanced consumption of H atoms. In lean H<sub>2</sub>/CO flames, the H atoms are extremely important as they control the main branching ( $\text{H} + \text{O}_2 \rightarrow \text{O} + \text{OH}$ ) and termination ( $\text{H} + \text{O}_2 + \text{M} \rightarrow \text{HO}_2 + \text{M}$ ) reactions. Since CO<sub>2</sub> dilution alters the H atom concentration, and consequently the chain branching and termination reactions, CO<sub>2</sub> can have profound effects on flame propagation and flame speeds of H<sub>2</sub>/CO flames. This effect is further pronounced at higher pressures, as the three-body termination reaction dominates, resulting in lower flammability limits on the lean side. Chemical kinetic studies have emphasized this point by comparing the flame speeds of mixtures with CO<sub>2</sub> dilution, and a fictitious chemically inert species with the same specific heat as CO<sub>2</sub>, showing that the CO<sub>2</sub> diluted flame speed had lower flame speeds (Zhu *et al.*, 1988).

The fourth effect of CO<sub>2</sub> dilution is through enhanced levels of radiation, as CO<sub>2</sub> is an effective absorber and radiator. CO<sub>2</sub> dilution can result in lower flame temperatures and lower laminar flame speeds (compared to air dilution) due to radiative losses from the flame (Qin *et al.*, 2001). Numerical studies in methane flames (Ruan *et al.*, 2001) have shown that the optically thin model loses effectiveness for large CO<sub>2</sub> dilution ratios and low equivalence ratios. Thus, CO<sub>2</sub> can also reabsorb the flame radiation and provide a means for heat transfer across greater regions of the flame.

Despite its importance, there is substantial scatter in the data of laminar burning velocities (see review by Andrews and Bradley, 1972; Egolfopoulos *et al.*, 1989) due to the difficulty in experimentally achieving planar, adiabatic, steady, unstrained laminar flames. Various methods have been adopted to determine laminar flame speed. One easily implemented approach is denoted the Bunsen burner method, i.e., a laminar, premixed jet flame. Another approach that has been reasonably successful for accurate  $S_L$  measurements is the counterflow technique (Wu and Law, 1984; Law, 1988) where a planar flame is established between two opposed jets. Using this technique, flame stretch effects can be systematically subtracted out to obtain un-stretched laminar flame speeds

In addition to the experiments, computational chemical kinetic studies are being used to identify appropriate chemical mechanisms to model synthetic gas mixtures under these conditions. With the experimental data and kinetic mechanisms, reduced chemistry and appropriate correlations can be used to capture flame propagation and premixed extinction limits as functions of fuel composition, strain rate, pressure and temperature.

In the current reporting period, we have tested four kinetic mechanisms. The first is mechanism is GRI Mech 3.0, a well-tested mechanism that has been validated extensively for methane chemistry, and therefore also includes oxyhydrogen and carbon monoxide mechanisms. The second mechanism that we chose is a mechanism developed recently for H<sub>2</sub>/CO combustion.

This mechanism (Davis *et al.*, 2004) is built on the kinetic model of Mueller *et al.* (1999) with rate parameters and efficiencies that have been revised over the last few years. This “full” mechanism involves 11 chemically reactive species (as well as various diluents) and 30 kinetic steps. The other two mechanisms were for this program by J. Y. Chen. They are reduced mechanisms: one uses 14 species, the other tracks only 9 species (which has significant advantages for CFD implementations).

In the last reporting period, LES computations were started that corresponded to flow evolution with species injection but without any reaction rate calculations. During the current period, combustion computations have been carried out in order to get a statistically better picture of the flow field, which are presented within this report.

#### **1.4 Task 4 (Systems Plant Performance Modeling)**

This task identifies critical plant level requirements by reviewing the DOE Co-generation plant program plan and EECF Phase 1 report. A Quality Flow Down (QFD) method is utilized to establish combustor level requirements flowing down from plant level requirements. This task provides combined cycle performance evaluations of various conceptual combustor designs to help downselect the combustor technologies for further development of a low emissions fuel flexible combustor. Results from the performance analysis are also used to determine the fuel flexible combustor operating conditions for operation in existing conventional gas turbine power systems. Details of the plant modeling of Task 4 were discussed in the July-December 2005 reporting period.

#### **1.5 Task 5 (Fuel Flexible Combustor Prototype Design)**

The purpose of this task is to design and fabricate two prototypes of a fuel flexible combustor and operate them in a single nozzle combustion test rig under heavy-duty gas turbine operating conditions. The prototypes were designed from the downselected technologies in Task-2 with operating conditions estimated from Task 4 results and current industrial gas turbine cycle conditions. This report discusses the design and performance for the second prototype, which is based on the Trapped Vortex Combustion technology adapted to syngas applications. The TVC combustor was developed under a different program for natural gas applications. The TVC combustor will be adapted to a syngas application and evaluated.

#### **1.6 Task 6 (Syngas Methodology for Advanced CFD tools)**

It is also important to develop the capability to apply the syngas information and kinetic mechanisms to complex combustor flows. Therefore, we have been developing CFD methodologies to explore extinction limit issues in practical combustors. Current studies include DNS and LES studies. The former is intended to examine the application of the reduced order mechanisms required for LES studies. The second study is intended to develop and explore capabilities to predict extinction phenomena in practical combustor geometries.

Flow features inside a gas turbine combustor are investigated by Large Eddy Simulation computations. The configuration and test conditions were provided by GE for this study. Special emphasis is placed on the mixing characteristics and the accurate representation of the chemical state space by reduced reaction mechanisms. LES computations are started on the exit plane of the diffuser cap and throughout the simulations injection of fuel and diluents from the holes are handled with special care. Results show that the effective mixing of fuel and oxidizer occur on the downstream due to the existence of a diluent stream and flame starts at this location. A recirculation zone exists on the inner section of the combustor which carries the hot products upstream and causes pre heating.

## Executive Summary

Current commercially available combustion system cannot meet the fuel flexible requirements targeted by this program, which are low emissions capability, multi-fuel flexibility, and fuel flexibility with respect to a wide range of heating values for syngas fuels. The goal of this program is to evaluate and improve upon existing leading combustor designs that can partially meet these requirements and to develop new technologies as appropriate to meet performance requirements and expand operability limits. The success and resultant quality of the fuel-flexible combustion system are enhanced by the Design for Six Sigma (DFSS) quality process, which is a statistically based methodology focused on flowing performance specifications and tolerances from the high level of customer or Co-production plant objectives down to the low level of component parts. The current process capability of each component flows back up to understand the influence of its variability on system performance. Using this methodology with a conceptual plant model and market driven inputs from Texaco will ensure that the combustion system is indeed flexible enough for highly efficient operation.

As a result of evaluating existing and advanced technology using the Six Sigma process, two concepts are selected that can meet the program performance requirements: prototype 1, a hybrid of a diffusion combustor for syngas and lean premixed swirl combustor for natural gas; and prototype 2, a trapped vortex combustor for both natural gas and syngas. The hybrid combustor successfully incorporates the low-NO<sub>x</sub> performance of GE's most advanced premixed combustion systems with a new version of an Integrated Gasification Combined Cycle (IGCC) diffusion nozzle for syngas fuels. This concept will provide a fuel-flexible combustor design capable of single-digit NO<sub>x</sub> and CO emissions, greatly enhanced fuel flexibility (100-280 BTU/scf), multi-fuel firing capability (syngas and natural gas for backup firing with low emissions), and co-firing capability as well. However, the unique challenges of low-NO<sub>x</sub> operation on high-hydrogen fuel, F-class operation of low Btu/scf fuels, and changing market demands, such as increased turndown or part load operation, may require the introduction and refinement of some of our most advanced technology. The Trapped Vortex Combustor was selected because its premixing of the syngas with the air and has the advantage of not being dependent on diluent addition for low emission performance. The technology builds upon GE's successful multi-year development of an Advanced Combustion System for Next Generation Gas Turbines DE-FC26-01NT41020 for natural gas combustion.

The effect of preheating and CO<sub>2</sub> dilution have been studied using a burner stabilized, stagnation flame configuration for a 50:50 H<sub>2</sub>:CO fuel mixture for which larger discrepancies have been observed between the previous Bunsen flame measurements and simulation results. Various preheat levels and equivalent ratios have been studied. Strain rates have also been measured in the flames. Four chemical kinetic mechanisms have been studied. Three of these mechanisms are reduced order mechanisms which can be applied to CFD modeling. The

predictions of these models is compared with experimental measurements of flame speed and strain rate.

The design of a trapped vortex combustor for syngas & natural gas operation is discussed in this report. The combustor has already demonstrated low emission performance at the targeted conditions with natural gas in the Advanced Combustion System for Next Generation Gas Turbines DE-FC26-01NT41020 research program. The hardware was modified for syngas operation in this program. The TVC combustor was operated with syngas for the first time during this reporting period.

A reduced order chemical mechanism has been applied to Prototype-1, they hybrid burner. The 14-species Chen mechanism was selected for this purpose. The time resolved flame position, fuel-mixing and turbulent quantities are all characterized by this modeling approach. The hybrid nozzle flow field and temperature field are described as well as the fuel burnout profiles.

## 2 Experimental

### 2.1 Task 3 (Syngas Fuel Flame Characterization)

#### 2.1.1 Apparatus

During the current reporting period, our experimental efforts have focused on strained flame measurements at elevated temperature, as the previous conical (Bunsen) flame results indicated that the mechanism greatest errors were at high reactant temperatures (>500-600 K, and therefore a relevant concern for gas turbine combustor modeling). The strained flame data were acquired in a stagnation flow configuration. This configuration, like the more common opposed flow, allows for stretch corrected  $S_L$  measurements of a one-dimensional flame. Furthermore, it is advantageous over the opposed flow arrangement for determining laminar flame speeds for the following reasons: (1) the use of a solid wall leads to more stable flames (Egolfopoulos *et al.*, 1997), (2) problems related to heating of the upper burner are eliminated, (3) since only one burner is used, fuel consumption is halved, and (4) ease of operation of a single jet especially at higher pressures.

A general schematic of the stagnation flow burner is shown in Figure 2.1-1. Fuel ( $H_2$ , CO and  $CO_2$  mixtures) and air flows are monitored with rotameters and the fuel/air mixture is premixed in the mixing section ahead of the burner. The burner is a smoothly contoured nozzle with the exit diameter (D) of either 6.25 or 9 mm and a contraction ratio of either 144 or 72. The purpose of having a contoured nozzle is to get a top hat velocity profile at the burner exit so that the flame stretch will be uniform throughout the flame area. Moreover, the high contraction ratio contoured nozzle ensures laminar flow even at high Reynolds number based on the burner exit diameter. Flow straighteners have been used before the contoured nozzle to remove any unsteadiness in the incoming flow. Care has been taken to reduce the size of the wake region created due to the finite thickness of the contoured nozzle at the burner exit.

A stainless steel plug was used to induce the stagnation zone. The plug was produced from a stainless steel rod (1.5" diameter), with the end first formed into a hemisphere. Then the end is removed to produce a small flat 0.5" long. The distance (L) between the burner exit and the stagnation plug can be adjusted depending on the burning velocity of the fuel mixture and the desired strain rate. As the burning velocity increases, decreasing the distance between the burner exit and the plug leads to a stable stagnation flame. In the current data, L/D was ~0.6-0.8. The burner exhaust is shielded by a quartz tube to prevent entrainment of ambient air, while allowing optical access for laser Doppler velocimetry (LDV) and flame imaging.

The reactants are preheated by electrical resistance tape wrapped around the burner. Once the desired reactant temperature is achieved (as determined by a type-K thermocouple,  $TC_1$ , placed at the center of the burner 1" below the exit), the surface temperature of the burner is monitored by a second thermocouple,  $TC_2$ , and held constant by a temperature controller. The mixture temperature at the exit of the burner has a nearly uniform radial profile ( $\Delta T \approx 3-5$  K).

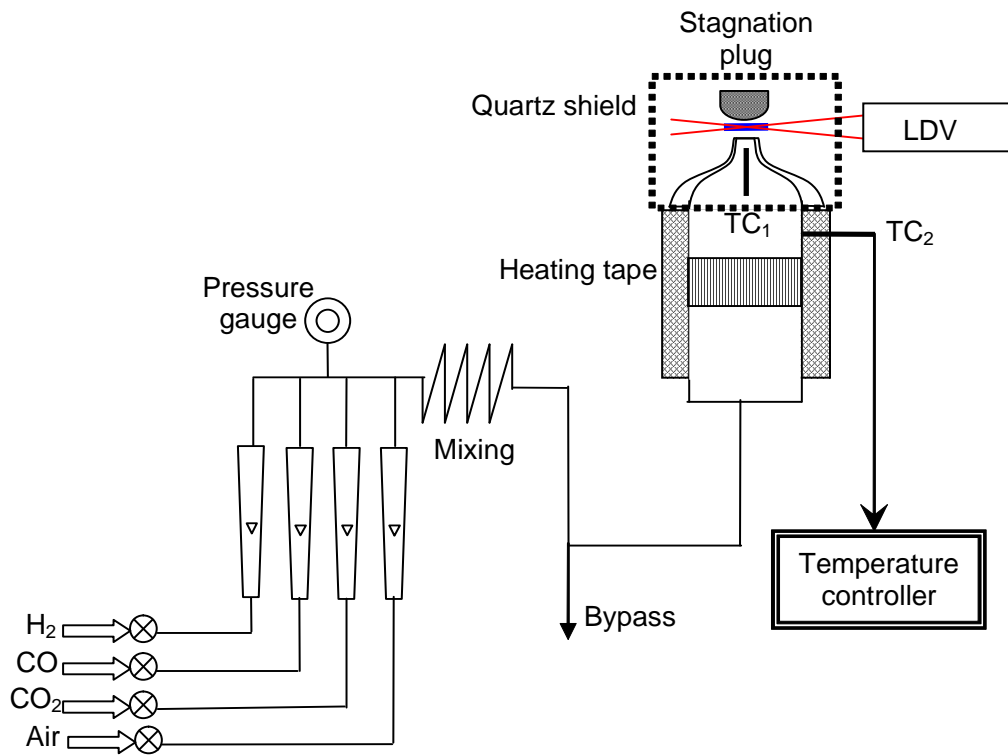


Figure 2.1-1: Schematic of stagnation flame burner.

## 2.1.2 Experimental and operating data

Figure 2.1-2 shows an image of the stagnation flame from the earlier high pressure measurements. The stagnation flames are extremely flat and stable at the center but slightly curved at the edges. The distance between the flame and stagnation plate varies from about 1 to 3mm, depending on the average inflow velocity. Figure 2.1-3 shows LDV velocity measurements. Results are shown for one fuel-air mixture and various flow velocities, i.e., different strain rates. The main flame zone occurs in the sharp velocity gradient region between the velocity minimum and the maximum to the left.

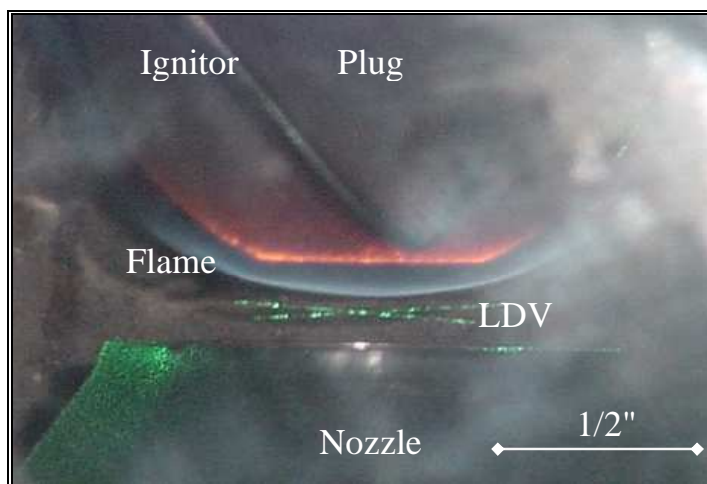


Figure 2.1-2: Image of flame emission from a stagnation flame at  $p=5.0$  atm for a fuel mixture  $H_2:CO=10:90$  at an equivalence ratio  $\phi=0.6$ ; average inflow velocity  $\sim 4S_L$ ;  $L/D=0.5$ .

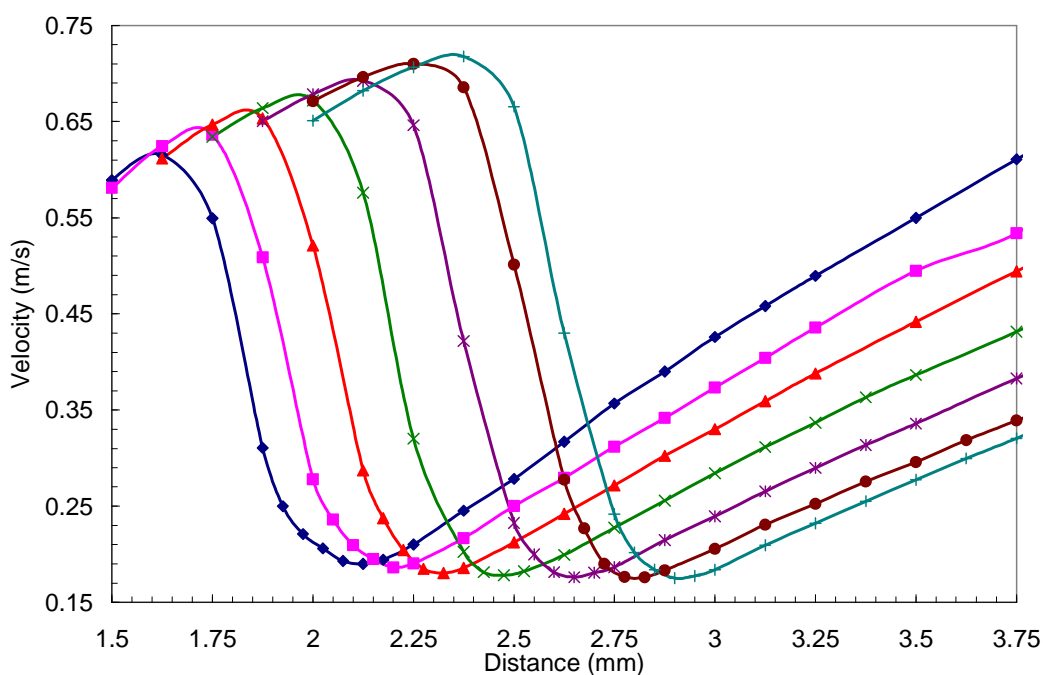


Figure 2.1-3: Velocity measurements along the centerline of a stagnation flame for 90% CO and 10%  $H_2$  fuel mixture,  $\phi=0.6$ ,  $p=5.0$  atm at seven flow rates. The flow direction is right to left in this figure, i.e., cold reactants are present at 3.75 mm, while there are hot products at 1.5 mm.

In addition, radial and axial velocities (not shown here) were measured for our unique burner stabilized stagnation flame configuration to make sure the flow remains one dimensional along the stagnation stream line and so that comparison can be made to the Chemkin OPPDIFF flame code predictions. The results indicate excellent agreement with the one-dimensional assumption along the centerline.

### 2.1.3 Data Reduction

The commonly employed definition of the strained (unburned) laminar flame speed in a 1-d stagnation flame is the velocity at the minimum condition seen in Figure 2.1-3. The strain rate is found by determining the velocity gradient in the unburned gases ahead of the minimum. Based on these definitions, raw data such as that shown in Figure 2.1-3 is reduced to a measure of laminar flame speed as a function of strain rate (see Figure 2.1-4). In this case, the extrapolated zero-strain laminar flame speed is nearly 15 cm/s.

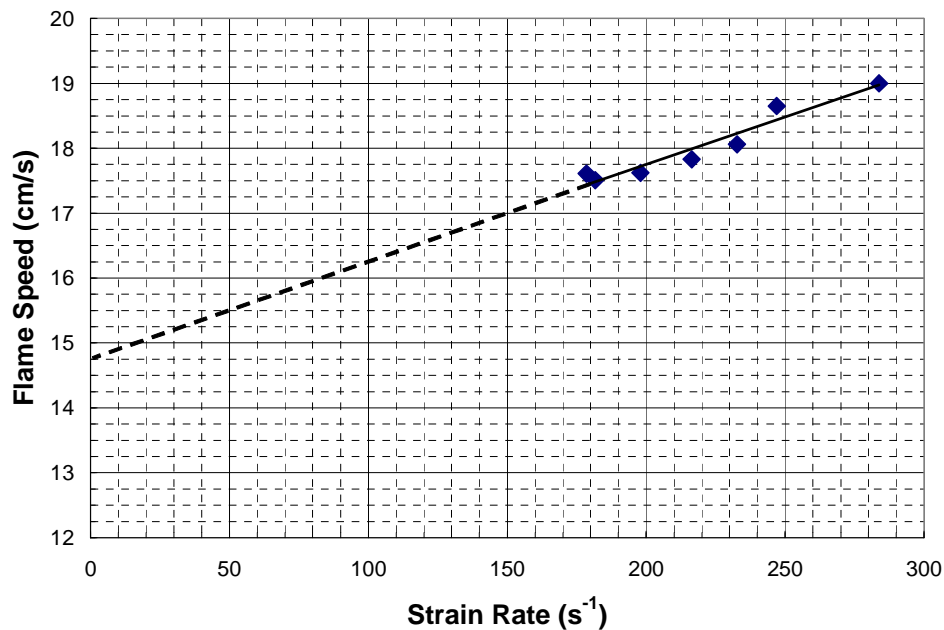


Figure 2.1-4: Measured flame speeds corresponding to results shown in Figure 2.1-3.

## 2.2 Task 5 (Prototype Design)

### 2.2.1 Trapped Vortex Combustor Design (Prototype-2)

Trapped vortex combustion (TVC) is one of the leading technologies for fuel flexible combustion as determined in Task 2 of this program. Research into the performance of trapped vortex combustors with natural gas was conducted in the Advanced Combustion System for Next Generation Gas Turbines DE-FC26-01NT41020 program. The scale of the combustor evaluated in that program is the same as the scale used here. Some of the components were passed on to this program at the completion of DE-FC26-01NT41020.

Several components of the TVC combustor were redesigned to facilitate operation with syngas. The cavity premixer was redesigned to handle the higher volumetric flow of the syngas.

The cavity air flow passage and the cavity fuel injection passages were appropriately resized for the higher volumetric flow associated with syngas. Downstream of this, a new cavity driver supply tube was designed with discrete fueling passages for the forward wall jets. The new tube maintains a higher flow velocity in the premixer for additional flashback protection. The main premixer was modified as well. The main mixer is comprised of a 3.5" schedule 10 pipe with static mixing elements. Additional mixing elements were added, bringing the total number to 7, to increase the level of mixedness between the air and the large volume of syngas. The additional elements were predicted to enable the mixer to perform at the level of entitlement. The entrance to the main burner ports was also modified to keep the syngas-air mixture moving at a higher velocity to better avoid flashback. The main burner port design was the same as was used in the previous program.

The cavity aft-wall utilized in impingement cooled approach. The wall was continuous and had no cooling slots or holes. The aft-wall shape was welded directly to the outer-wall and combustion liner, and the wall was constructed from 2 sheets welded together. The flat part of the wall was a machined disk; the nose was custom machined. The aft-wall was backside cooled. The shroud cooling hole size and distribution were determined by the local wall heat transfer coefficients. The offset of the shroud was determined by the design analysis.

The outer-wall and transition piece were cooled in the same manner as the aft-wall. The cooling shroud extended from the forward end of the outer wall to the start of the hula seal. The combustion air was directed through cooling holes by designing a seal between the premixers and the reverse flow liner. In this manner air was forced to travel through the cooling shroud before passing into the combustor.

Effective area tests were performed to determine the air splits in the regions of the combustor shown in Figure 2.2-2. Region A is leakage air between the hula seal on the combustion liner and the downstream combustion liner (not pictured). Region B is cooling air used to cool the metal wall temperatures of the combustion liner. Region C is air that passes through the cavity premixer and cavity slots into the cavity zone of the combustor. Region D, passes through the main premixing section and main slots in the main zone of the combustor. Region E is effusion cooling air used to cool the surface of the combustion injector plate, which is also referred to as the forward wall.

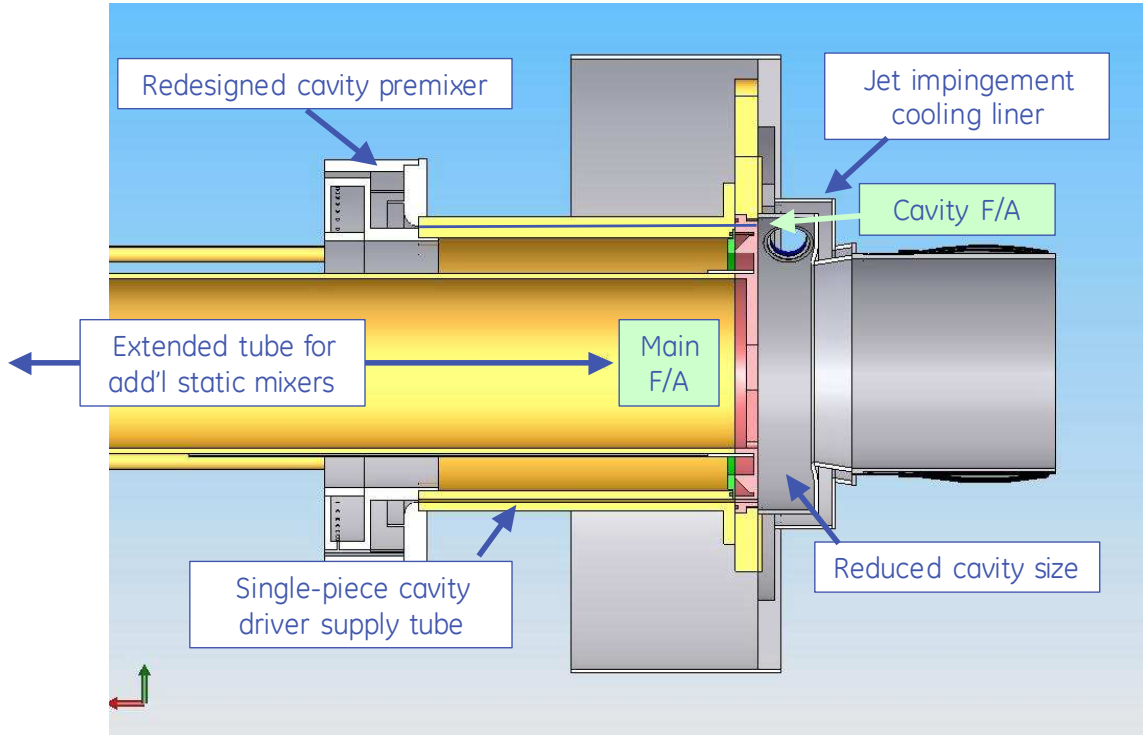


Figure 2.2-1: Prototype-2 TVC Combustor Design Features

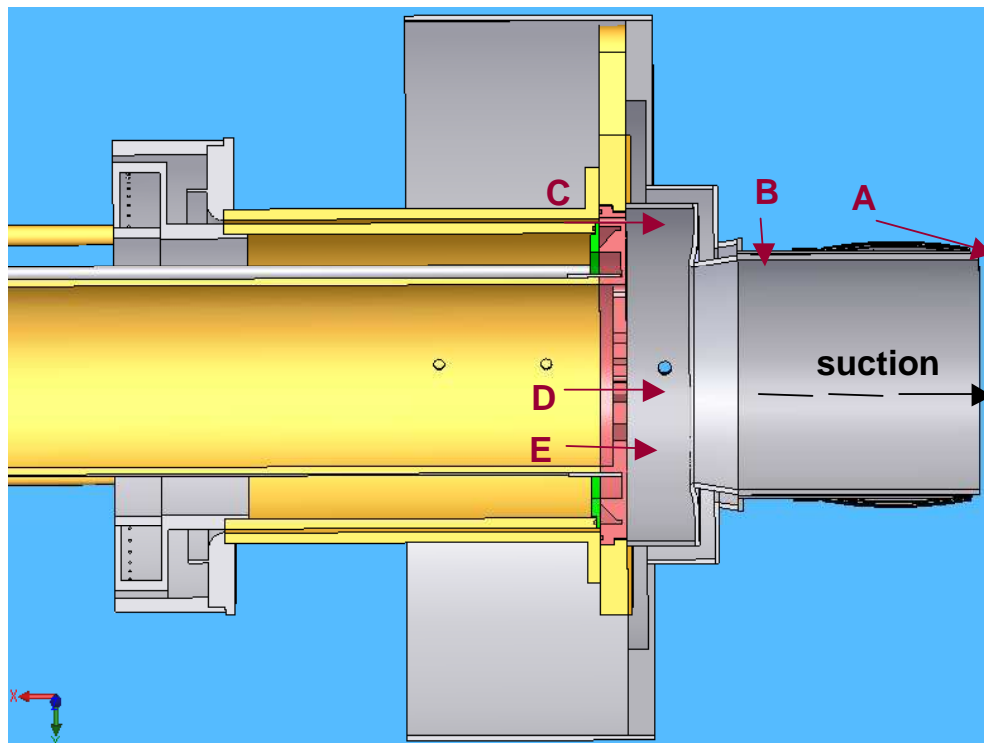


Figure 2.2-2: Prototype-2 Air Flow Passages

## 2.2.2 Instrumentation

Thermocouple locations for Prototype-2, trapped vortex combustor, are shown in Figure 2.2-3. Thermocouples were used to monitor conditions of state, detect flashback, and measure. The inlet air temperature before and after the cooling liner is measured. Inside the cavity three TC's were located in the mixing chamber and three in the deriver supply tube. Three TC's were also located in the main premixer. Wall temperatures were measured on the main mixing ports, the forward wall, outer wall, aft wall and corner. Representative data of these surface temperatures is given in Section 3.3.

Pressure tap locations are shown in Figure 2.2-4. These are used to monitor conditions of state, estimate velocities, and monitor hardware conditions. Location P8 was used to monitor combustor pressure as well as P6 and P7. P2-P3 measured cooling pressure drop, and P3-P8 measured combustor pressure drop. In addition, dynamic pressure measurements were taken at pressure locations numbered 6,7, and 8 in the figure depicting the main combustion region, the cavity combustion region, and the combustion liner region of the test stand.

Figure 2.2-5 shows a downstream view of the TVC hardware. The figure shows the exit of the combustor, which is covered with the hula seal that connects to the downstream combustion liner during assembly. Also shown is the cavity impingement cooling sleeve and some of the instrumentation on the exterior of the hardware. The impingement cooling sleeve keeps the walls of the combustor cool during operation. Figure 2.2-6 is a close up of the water-cooled igniter protruding through the impingement cooled liner and placed flush against the wall of the cavity combustor.

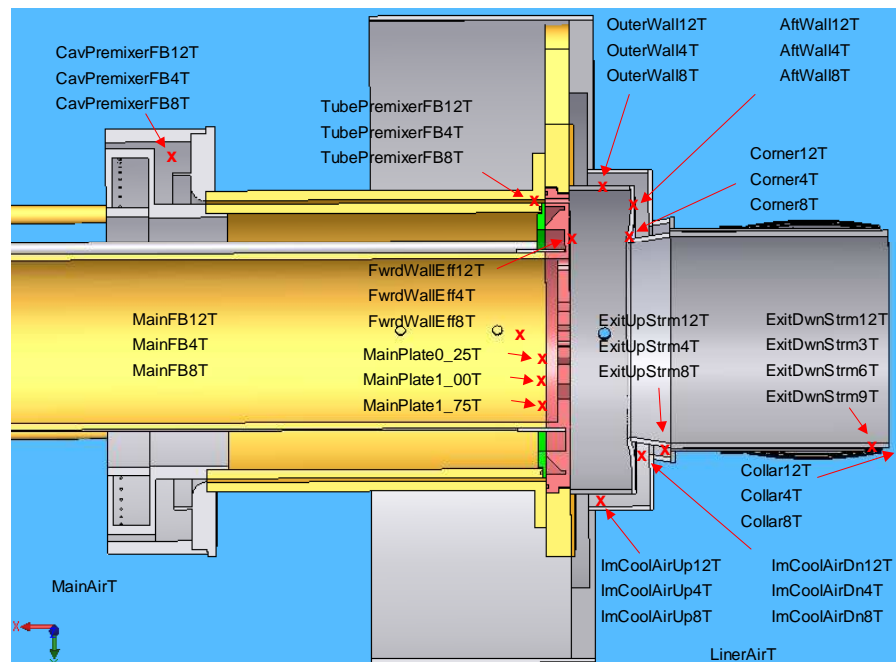


Figure 2.2-3: Prototype-2 Thermocouple Locations

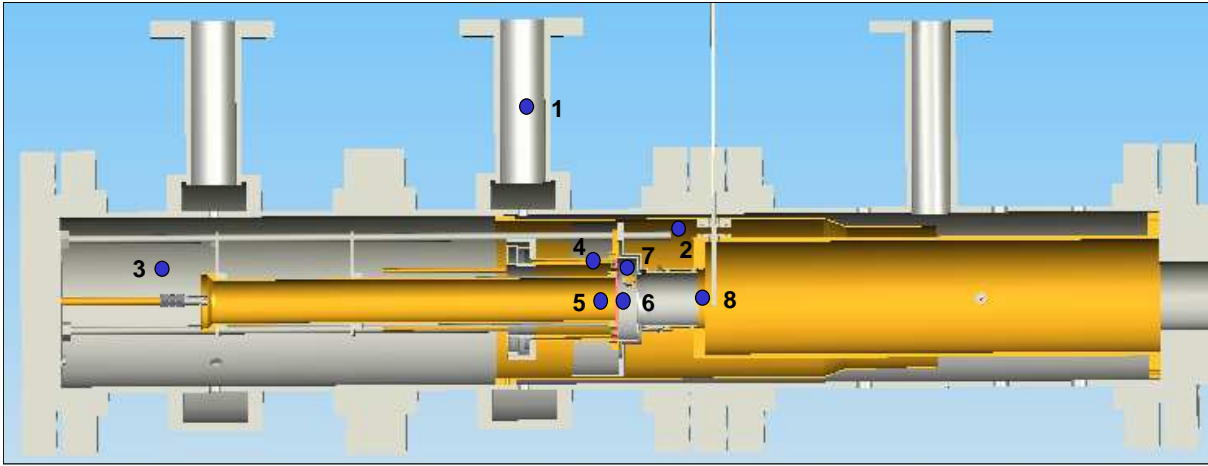


Figure 2.2-4: Prototype-2 pressure instrumentation nomenclature and locations

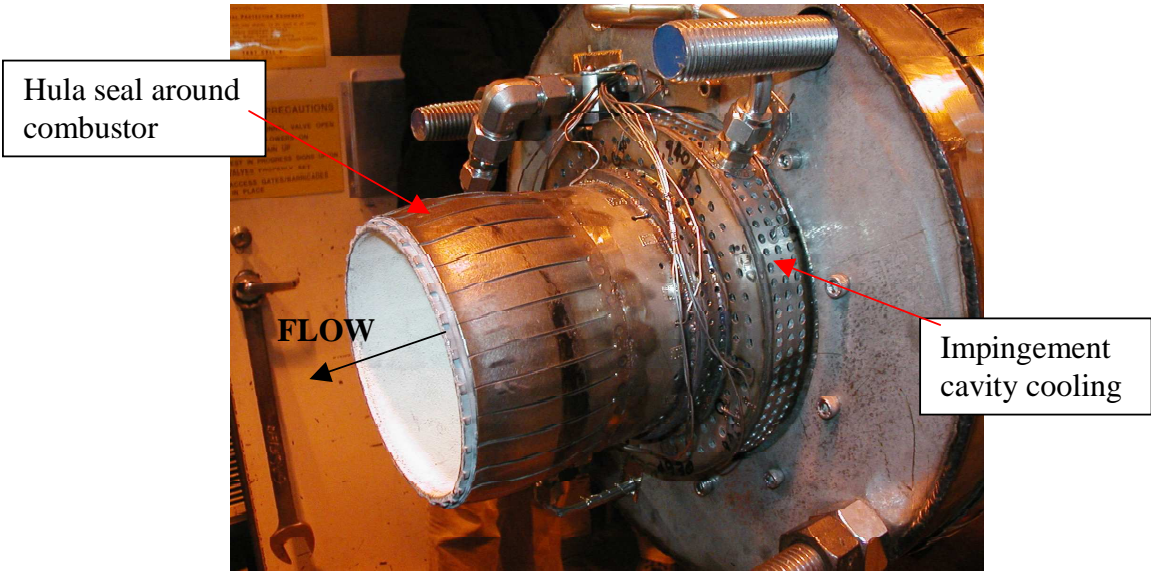


Figure 2.2-5: Prototype-2 Hardware

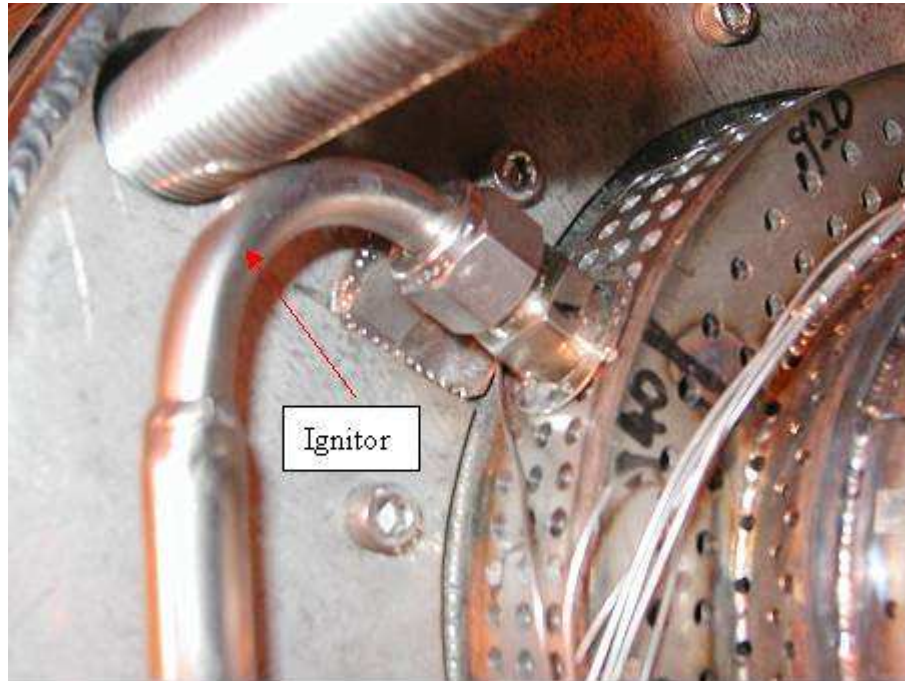


Figure 2.2-6: Prototype-2 water-cooled, hydrogen spark igniter located through impingement cooling sleeve and aft wall of the combustion cavity section

## 2.3 Task 6 (Advanced CFD tools)

### 2.3.1 Apparatus

#### 2.3.1.1 Syngas Methodology for Advanced CFD tools

Accurate prediction of the scalar and velocity fields inside the combustion chamber of a practical gas turbine engine is a challenging task in that it requires the solution of a 3 dimensional, highly unsteady turbulent reactive flow. Even though there are reliable models for the flow (Pope, 2000) and chemistry (Pope, 1997 and Maas and Pope, 1992) alone, interaction of these processes with each other still remains as a task which needs to be studied further. In the first half of this year we employed direct numerical simulations (DNS) to study flame-turbulence interactions using relatively detailed reaction kinetics for syngas. These studies confirmed the integration of the models within our solver. However, for the full scale combustor, DNS is not feasible and therefore, we employ large-eddy simulation (LES) to study this flow.

Large Eddy Simulation (LES) methodology has been employed here as the computational tool for reactive flows. In LES, scales larger than the grid size are computed directly and smaller scales are modeled (Menon and Calhoon, 1996 and Kim *et al.*, 1999). Current efforts focus on

the use of LES to predict flow inside gas turbine combustors. LES has been studied extensively for different combustion regimes in realistic (Sankaran and Menon, 2004, Pitsch, 2005 and Mahesh *et al.* 2000), and simplified geometries (Kempf *et al.*, 2006), for which it is possible to get experimental data (Weigand *et al.*, 2006, Meier *et al.*, 2006 and Meyer *et al.*, 2005) for validation purposes.

As oversimplified (e.g., single-step) global reaction models are not expected to be reliable to predict the flame dynamics over a wide range of operating conditions, our work also involves evaluation of multi-step, but reduced kinetic mechanisms designed especially for CO-H<sub>2</sub> combustion. In the previous (and current) period, a 10-step, 14-species mechanism was evaluated. In the current period, we have also tested a 5-step, 9-species mechanism and employed these mechanisms in an LES computation. The LES computation was performed on the combustor geometry that was provided by GE Global Research. All test conditions for the LES were chosen from the data provided by GE researchers. Results described in this report are still preliminary in some respects, since these simulations take time to complete and to obtain statistical stationary data for analysis. Nevertheless, some interesting observations can be made from the current data.

### 2.3.1.2 LES Mathematical Formulation

The LES equations are obtained by using a top hat filtering operation of the Navier Stokes equations and the following resultant equations for continuity, momentum, total energy and species conservation are obtained:

$$\frac{\partial \bar{\rho}}{\partial t} + \frac{\partial \bar{\rho} \tilde{u}_i}{\partial x_i} = 0 \quad (2.5.1)$$

$$\frac{\partial \bar{\rho} \tilde{u}_i}{\partial t} + \frac{\partial}{\partial x_i} \left[ \bar{\rho} \tilde{u}_i \tilde{u}_j + \bar{p} \delta_{ij} - \bar{\tau}_{ij} + \tau_{ij}^{sgs} \right] = 0 \quad (2.5.2)$$

$$\frac{\partial \bar{\rho} \tilde{E}}{\partial t} + \frac{\partial}{\partial x_i} \left[ (\bar{\rho} \tilde{E} + \bar{p}) \tilde{u}_i + \bar{q}_i - \tilde{u}_j \bar{\tau}_{ji} + H_i^{sgs} + \sigma_{ij}^{sgs} \right] = 0 \quad (2.5.3)$$

$$\frac{\partial \bar{\rho} \tilde{Y}_m}{\partial t} + \frac{\partial}{\partial x_j} \left[ \bar{\rho} \tilde{Y}_m \tilde{u}_j + \bar{\rho} \tilde{D}_m \frac{\partial \tilde{Y}_m}{\partial x_j} + \Phi_{jm}^{sgs} + \Theta_{jm}^{sgs} \right] = \bar{\rho} \tilde{\omega}_m \quad (2.5.4)$$

Here,  $\sim$  represents Favre averaging operator and is calculated for a given quantity  $\tilde{f}$  as  $\overline{\rho f} / \bar{\rho}$ , where the over bar stands for volume averaging. Filtering operation introduced new terms into the set of governing equations and they represent the effect of the scales smaller than the grid size, on the resolved variables. These terms are denoted with the sgs superscript and are, the sub-grid shear stress tensor  $\tau_{ij}^{sgs} = \bar{\rho} \left[ u_i u_j - \tilde{u}_i \tilde{u}_j \right]$ , sub-grid heat flux  $H_i^{sgs} = \bar{\rho} \left[ E u_i - \tilde{E} \tilde{u}_i \right] + \left[ \overline{p u_i} - \bar{p} \tilde{u}_i \right]$ , sub-grid viscous stress  $\sigma_i^{sgs} = u_j \tau_{ji} - \tilde{u}_j \bar{\tau}_{ji}$ , sub-grid mass

flux  $\Phi_{jm}^{sgs} = \bar{\rho}[Y_m u_j - \tilde{Y}_m \tilde{u}_j]$ , and sub-grid diffuse mass flux  $\Theta_{jm}^{sgs} = \bar{\rho}[Y_m V_{jm} - \tilde{Y}_m \tilde{V}_{jm}]$ , respectively.

Total energy is given as  $\tilde{E} = \tilde{e} + \frac{1}{2}(\tilde{u}_k \tilde{u}_k) + k^{sgs}$  and the filtered pressure is calculated by the filtered equation of state by neglecting the effect of the sub-grid scale temperature as  $\bar{p} = \bar{\rho} R \tilde{T}$ , where  $\tilde{e}$  is the filtered internal energy,  $k^{sgs}$  the sub-grid scale kinetic energy and R gas constant.

### 2.3.1.3 LES Subgrid Closure Methods

Since the major effect of the small scales is to provide dissipation for the energy cascade from large scales through the inertial range, an eddy viscosity type sub-grid model appears to be suitable for the calculation of sub-grid stresses, heat flux and species flux. Based on this formulation spatial and temporal evolution of the sub-grid kinetic energy  $k^{sgs}$  is required in order to evaluate the eddy viscosity coefficient and the unclosed sub-grid scale terms. For this purpose an additional transport equation for  $k^{sgs}$  have been solved which is in the form of;

$$\frac{\partial \bar{\rho} k^{sgs}}{\partial t} + \frac{\partial}{\partial x_i} (\bar{\rho} \tilde{u}_i k^{sgs}) = P^{sgs} - D^{sgs} + \frac{\partial}{\partial x_i} \left( \frac{\bar{\rho} v_t}{Pr_i} \frac{\partial k^{sgs}}{\partial x_i} \right) \quad (2.5.5)$$

Here,  $P^{sgs}$  represents the production term and  $D^{sgs}$  is the dissipation term, and are given

as;  $P^{sgs} = -\tau_{ij}^{sgs} \frac{\partial \tilde{u}_i}{\partial x_j}$  and  $D^{sgs} = c_\epsilon \bar{\rho} \frac{(k^{sgs})^{3/2}}{\Delta}$ , respectively. Based on these theoretical

assumptions, sub-grid scale terms are closed as;

$$\tau_{ij}^{sgs} = -2\bar{\rho} v_t \left( \tilde{S}_{ij} - \frac{1}{3} S_{kk} \delta_{ij} \right) + \frac{2}{3} \bar{\rho} k^{sgs} \delta_{ij} \quad (2.5.6)$$

$$H_i^{sgs} = -\bar{\rho} \frac{v_t}{Pr_i} \frac{\partial \tilde{H}}{\partial x_i} \quad (2.5.7)$$

The sub-grid eddy viscosity is then obtained as  $v_t = c_v (k^{sgs})^{2/3} \bar{\Delta}$ . Within this formulation there appears two coefficients,  $c_\epsilon$   $c_v$ , whose values are taken 0.067 and 0.916 as constants at present, even though a dynamic approach to evaluate these coefficients exist. We plan to switch to the dynamic approach at a latter stage when the solution is well established. LES governing equations as are solved using a finite-volume scheme that is nominally second-order accurate in space and time. A fourth-order accurate scheme is also available, which will be used for the final set of simulation during data acquisition for statistical analysis. All simulations are conducted in parallel using MPI on Intel PC cluster.

## 3 Results and Discussion

### 3.1 Task 3 (Syngas Fuel Flame Characterization)

#### 3.1.1 Model Comparisons: Effect of Preheating and CO<sub>2</sub> Dilution

As indicated above, the primary goal of the experimental effort in the current reporting period was characterization of high temperature syngas flame speeds for comparison to chemical kinetic models for use in the CFD simulations. Four kinetic mechanisms (GRI Mech 3.0, the H<sub>2</sub>/CO mechanism of Davis *et al.* and two reduced order mechanisms of J Y Chen: a 14 species and a 9 species model) were studied. The laminar stagnation flame was simulated using the Chemkin OPPDIF flame code with appropriate detailed transport properties. It is important to note that in all our flame modeling *multi-component diffusion and thermal diffusion (Soret) effects are included*. These effects have a significant influence on the predicted flame properties especially at high preheat temperatures.

In the OPPDIF flame simulation, there are two premixed flames on either side of the stagnation plane and hence the stagnation surface is truly adiabatic. Moreover at the stagnation plane, the radial velocity gradient is normally considered finite. In our experiments, which use a solid wall at the stagnation plane, potential issues arise. First, it imposes a zero radial velocity gradient. Second, there is some amount of heat loss to the plug. Hence the effect of downstream heat loss and zero radial gradient at the stagnation surface have been studied and the results (not shown here) indicate that the unburned strained flame speed is not affected if the flame is located at least two flame thickness away from the stagnation surface. Thus in all our experiments care has been taken to stabilize the flame sufficiently away from the wall.

##### 3.1.1.1 Effect of Preheat: Strained Laminar Flame Speed Measurement

The wall stagnation flame method was used to measure the strained flame speed for the 50:50 H<sub>2</sub>:CO fuel mixture at high preheat temperatures (600 K and 700 K) and lean equivalence ratios (0.6 and 0.8) where larger discrepancies have been between the Bunsen flame measurements and the PREMIX flame model predictions (as reported in our earlier report). Due to the high flame speeds of these mixtures and the need for significant hydrodynamic strain rate to achieve a stable flame, the smaller nozzle diameter 6.25 mm with a nozzle-wall separation distance of 5 mm was used. Figure 3.1-1 shows the measured strained flame speeds for this composition at 600 K preheat temperature for 0.8 equivalence ratio. The measured flame speed increases with increasing strain rate, which indicate the negative Markstein length for the unburned flame speed. It should be noted that though the calculated strained flame speed increases linearly with the imposed strain rate, the unstrained flame speed found by linearly extrapolated to zero strain rate does not converge to the one dimensional laminar flame speed predicted by the Chemkin PREMIX code. A difference of as much as 10% has been observed for these conditions. Hence it is more appropriate to compare the measured strained flame speed with that predicted with the OPPDIF code. Figure 3.1-1 also shows the OPPDIF predictions for 0.6 and 0.8 equivalence ratios in the same strain rate range as that of experiments for all four mechanisms. As observed with the Bunsen flame measurements, both detailed mechanisms (GRI Mech 3.0 and the H<sub>2</sub>/CO mechanism of Davis *et al.*) slightly over predict the measurements. The

reduced 14 species mechanism is in good agreement with the measurements while the 9 species mechanism over predicts the measurements by 10%.

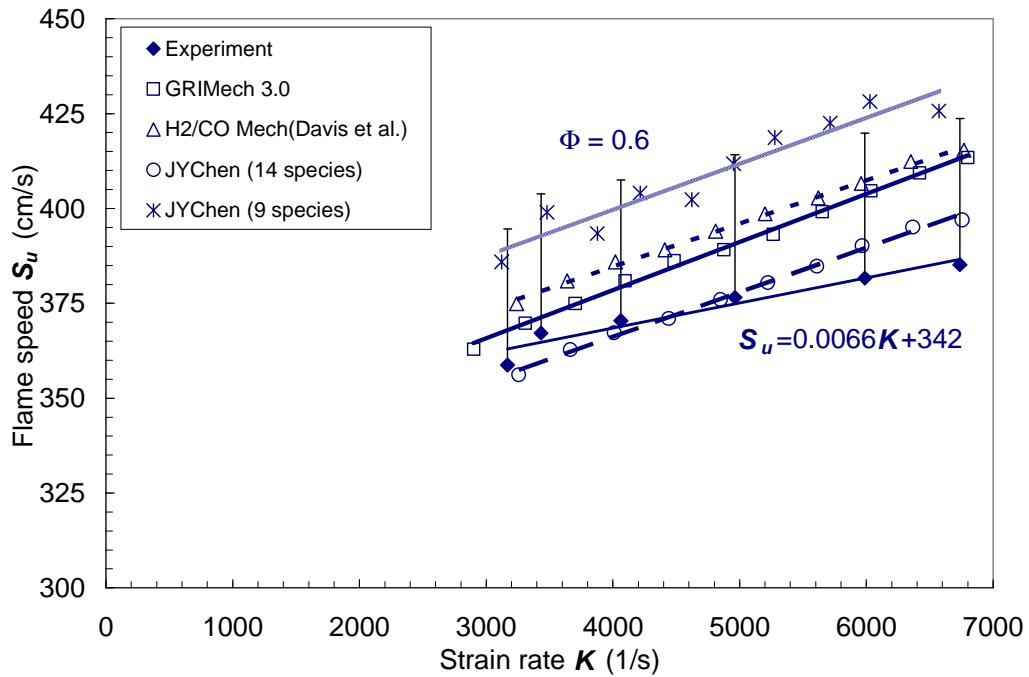


Figure 3.1-1 Flame speeds for a 50:50 H<sub>2</sub>:CO composition at 600 K preheat temperature for 0.6 equivalence ratios. (vertical bars on measurements indicate a 10% deviation band - not uncertainties in the measurements.)

Figure 3.1-2 shows the measured strained flame speeds for the same 50:50 H<sub>2</sub>:CO composition at 700 K preheat temperature for 0.6 and 0.8 equivalence ratios. The measured strained flame speed increases with the imposed strain rate linearly for both equivalence ratios. It is important to note that the flame at 0.6 equivalence ratio ( $\phi$ ) is more strain sensitive than at  $\phi=0.8$ . Figure 3.1-2 also shows the OPPDIF predictions for  $\phi=0.6$  and 0.8 in the same strain rate range as that of experiments for all four mechanisms. It can be observed from the Figure 3.1-2 that again the model results with all four mechanisms over predict the measurements. The Chen 14 species mechanism is again closest to the measurements, while the 9 species mechanism over predicts the measurements by more than 10%. As the equivalence ratio is reduced to 0.6, the difference between the measurements and the model predictions increases, which is qualitatively similar to our Bunsen flame measurement results. Predictions with GRI Mech 3.0 and the Chen 14 species mechanism is very similar, and they over predict the measurements by 10%. However the H<sub>2</sub>/CO mechanism of Davis *et al.* and the Chen 9 species mechanism over predict the data by 15% and 20% respectively.

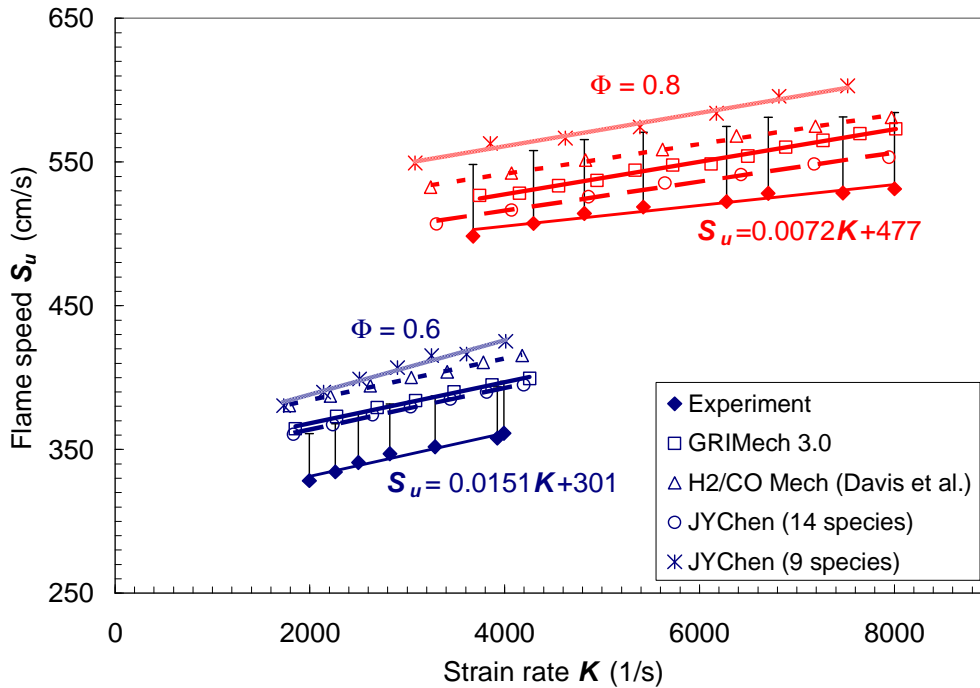


Figure 3.1-2 Flame speeds for a 50:50 H<sub>2</sub>:CO composition at 700 K preheat temperature for two equivalence ratios. (vertical bar on measurements indicate 10% deviation from the data. It is not the error in measurement).

### 3.1.1.2 Effect of Preheat and Dilution: Strained Laminar Flame Speed Measurement

The effect of CO<sub>2</sub> dilution at 700 K preheat temperature was studied for the 50:50 H<sub>2</sub>:CO mixture with 40% CO<sub>2</sub> dilution, which also resembles the syngas composition of interest to the full-scale plant. The appropriate nozzle diameter and the nozzle wall separation distance used for these measurements are 9 mm and 6 mm respectively. Figure 3.1-3 shows the measured strained flame speeds for this composition at 700 K preheat temperature for 0.6 and 0.8 equivalence ratios. At  $\phi=0.8$ , both GRI Mech 3.0 and the Chen 14 species mechanism over predict the measurements by 10% while the H<sub>2</sub>/CO mechanism of Davis *et al.* and the reduced Chen 9 species mechanism over predict the measurements by 15%. For the lower equivalence ratio to 0.6, the trends remain the same for the GRI Mech 3.0 and 14 species Chen mechanisms. However, the 9 species Chen mechanism over predicts the measurements by as much as 18%. Comparing the undiluted 50:50 H<sub>2</sub>:CO mixture measurements with the diluted case indicates that the spectral radiation reabsorption of CO<sub>2</sub> dilution does not make significant changes, in the agreement between the models and experiments.

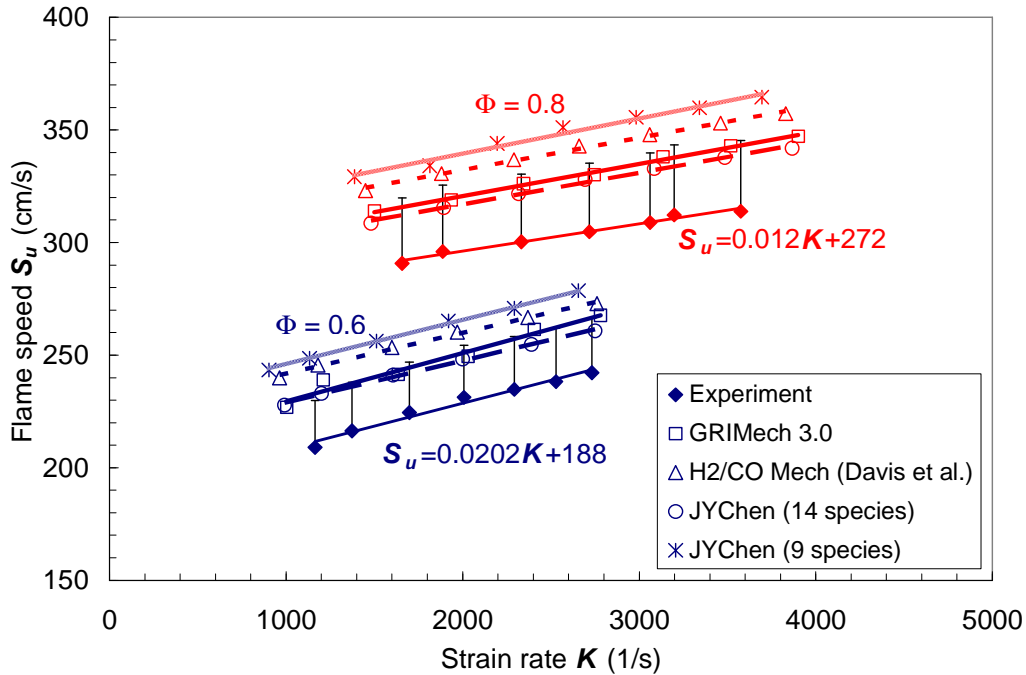


Figure 3.1-3: Flame speeds for a 30:30:40 H<sub>2</sub>:CO:CO<sub>2</sub> composition at 700 K preheat temperature for two equivalence ratios. (vertical bar on measurements indicate 10% deviation from the data. It is not the error in measurement).

## 3.2 Task 5 (Prototype Design)

### 3.2.1 Trapped Vortex Combustor (Prototype-2) Experimental Results

The trapped vortex combustor was operated with a representative EECP syngas fuel for the first time during this reporting period. The redesigned combustor components described previously were needed to prevent flashback into the premixers. During the initial evaluation no flashback events were encountered, and the premixers performed in accordance with the design intent despite the presence of Hydrogen. The syngas fuel was composed of 24% Hydrogen, 65% Nitrogen, and 11% methane. The hydrogen content was representative of the levels seen in the EECP fuels, and methane was added to the mixture to keep the overall heating value of the fuel in line with the EECP fuel spec.

The combustor was lit in a natural gas mode, and then operation was changed to a syngas-only mode of operation. Measurements of the combustor performance with syngas only are shown in the Figures below. Figure 3.2-1 shows the temperatures of interest during a representative time. The syngas-air mixture has a temperature of around 600 F as shown in the Figure. The combustor wall temperatures reflect the impact of cooling on the metal temperatures. The outer wall and forward wall are the coolest surfaces falling below 1100 F. The aft wall is somewhat hotter from the stagnation of

flow on the surface, but temperatures remained below 1300 F. The combustor corner is the hottest region of the combustor. With temperatures below 1700 F at the corner, the overall cooling design was deemed sufficient for prototype evaluation.

Combustion dynamics were measured at three different locations in the combustor as described in Section 2.2. Figure 3.2-2 shows the dynamics pressure measurements over the same period as the temperature measurements. The quiet performance of the combustor is clearly seen from the data. Peak dynamic pressure measurements were around 0.5 psi. The pressure tap at the main port shows very little response and the measurements in the cavity are weaker than those measured downstream, PCB8. The low dynamics in the TVC combustor is consistent with other experimental evaluations. The performance with syngas proved to be even more stable than with natural gas. Lower Btu fuels will also be explored for dynamics stability later in the program.

Figure 3.2-3 shows the measured levels of O<sub>2</sub> and CO<sub>2</sub> in the exhaust. The CO<sub>2</sub> is the product of methane combustion. The O<sub>2</sub> levels are below the ambient level of 21% due to the combustion of the Hydrogen and methane in air. Oxygen levels as low as 15% were produced at the hottest conditions and CO<sub>2</sub> levels of 1.5% were produced at this level. This is far below the CO<sub>2</sub> levels that are produced with hydrocarbon based fuels.

Figure 3.2-4 shows the NO<sub>x</sub> emission corrected for 15% O<sub>2</sub> levels during the same period of operation as above. The NO<sub>x</sub> measured NO<sub>x</sub> levels were less than 5 ppm. This is an encouraging result. It demonstrates that the premixers were successfully mixing the syngas with air without flashback during operation, and reactions were taking place in a premixed manner. The presence of a diffusion flame would have led to much higher NO<sub>x</sub> levels in the combustor. This result paves the way for further low emission studies for the trapped vortex combustor with syngas.

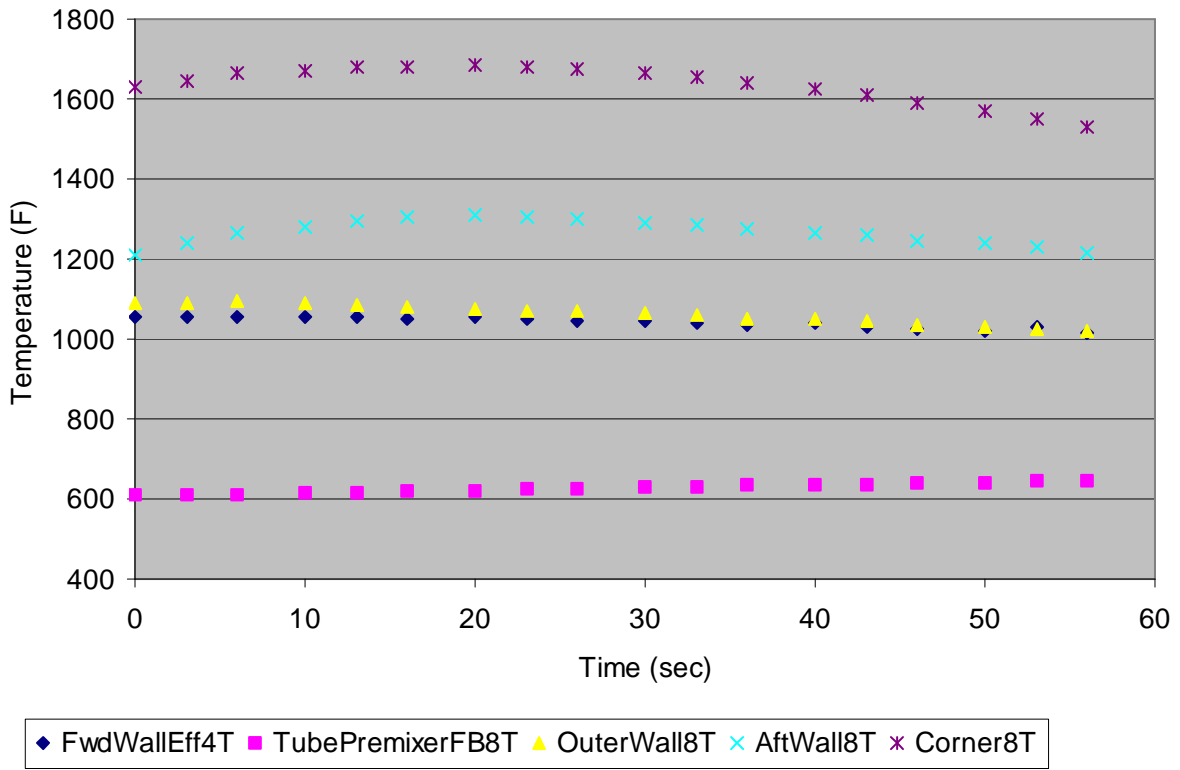


Figure 3.2-1: TVC Surface Temperatures with Syngas Combustion

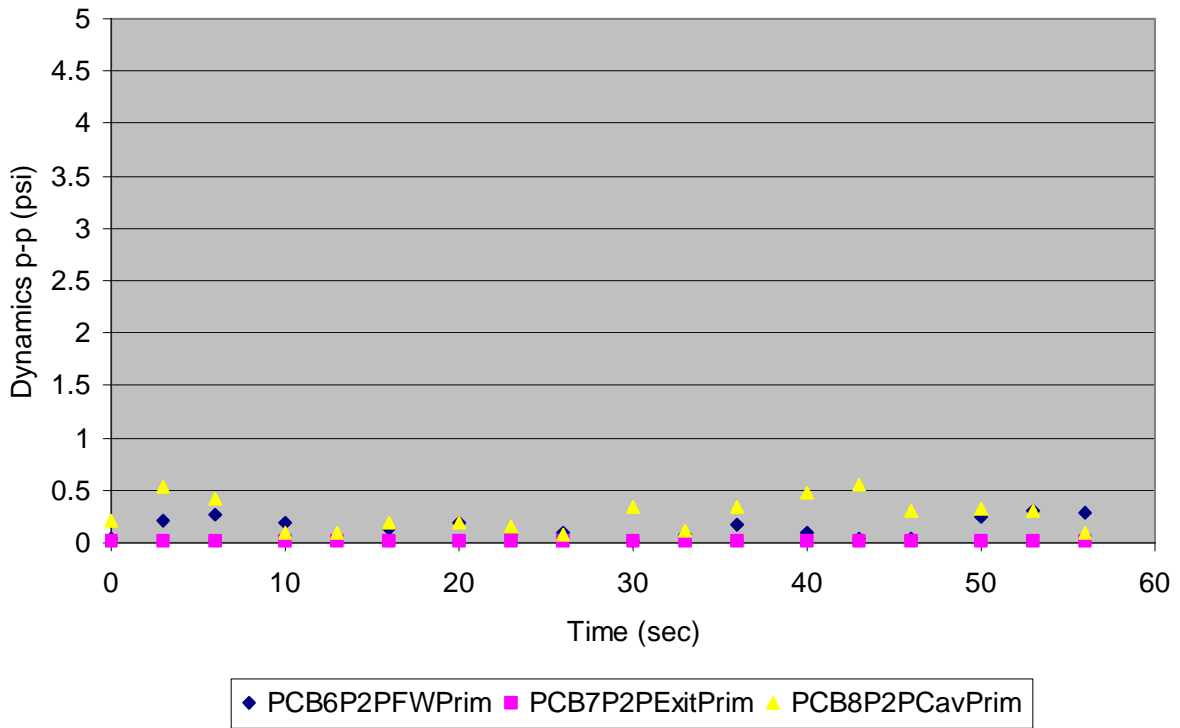


Figure 3.2-2: TVC Dynamics Measurements with Syngas

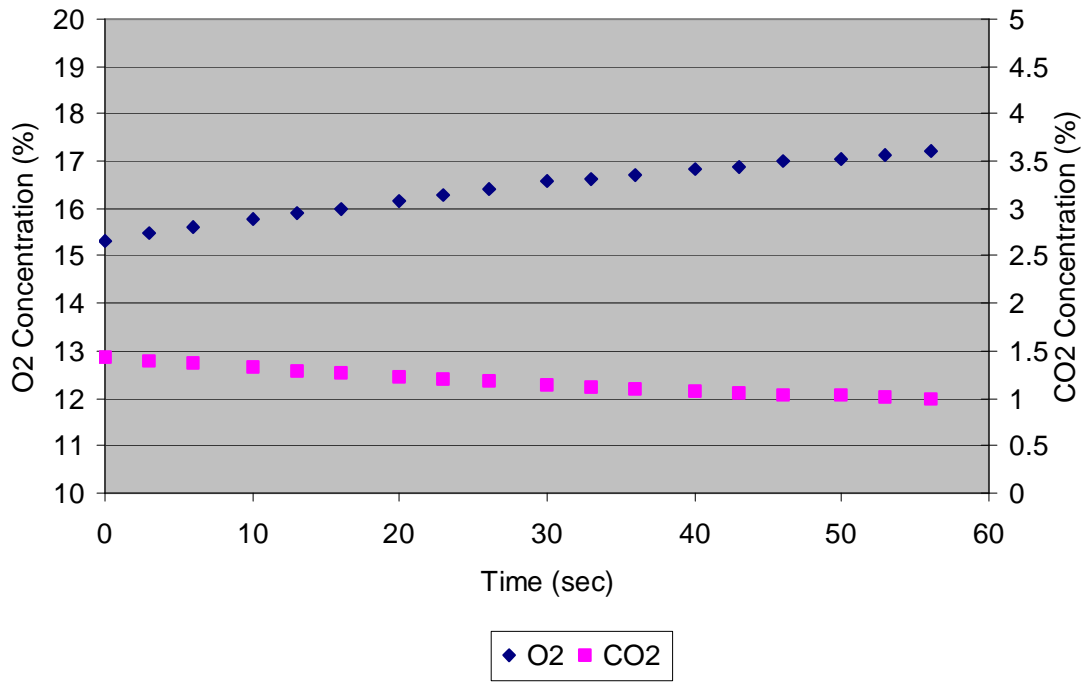


Figure 3.2-3: TVC Exhaust Oxygen and CO2 Concentrations with Syngas

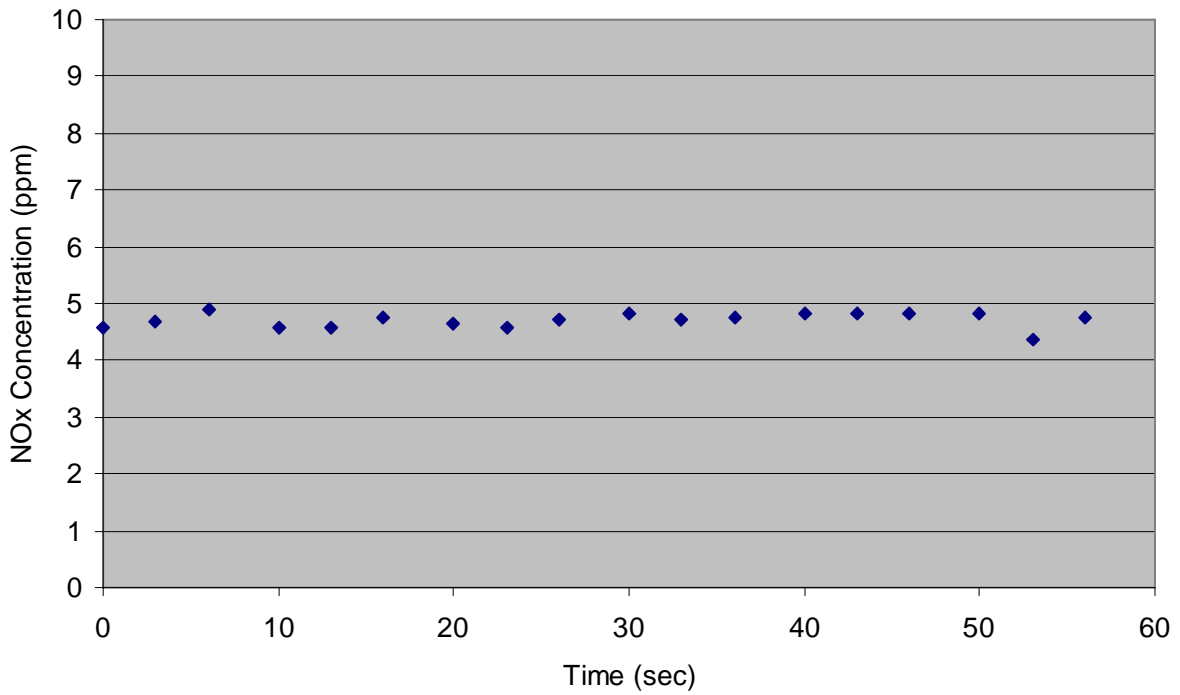


Figure 3.2-4: TVC NOx Emission with Syngas

### 3.3 Task 6 (Syngas Methodology for Advanced CFD Tools)

#### 3.3.1 Chemical Mechanism Validation

FVI performance comparison of the reduced mechanisms is given in Figure 2.1-1. Computations are performed in a rectangular box with the principle dimensions of  $0.02 \times 0.0075 \times 7.12 \cdot 10^{-5} \text{ m}^3$  where the third dimension is very small in order to restrict ourselves into a 2D problem. Fuel composition is 50:50  $\text{H}_2$ :CO without any dilution and with an equivalence ratio of 0.6. Velocity and pressure field inside the domain is initialized by PREMIX results obtained for the same fuel composition, equivalence ratio and are altered by the superposition of pair of counter rotating vortex pair. Maximum vorticity is chosen to be 31000 1/s, with a maximum velocity of 14 m/s, and the core diameter is 5.7 mm.

Comparison of the u velocities obtained at two different locations and by using two kinetic mechanisms was shown in the previous report. Here, our aim is to demonstrate the differences between the scalar fields obtained by using both mechanisms. Snapshots of the vorticity surface plot superimposed on the reaction rate contour plot of OH is given in Figure 3.3-1 at two instants,  $t=0.51$  and 1.02 msec. In this simulation, non-unity Lewis numbers are used, which is crucial for synthetic gaseous fuel mixtures as it has a very light ( $\text{H}_2$ ) and a relatively heavier species (CO) as fuel. The general picture suggests that the straining imposed by the Lamb dipole is high enough that it survived through the flame and tore a portion of the flame; a pocket full of fresh unburnt gases is seen. This phenomenon is reproduced by both of the reduced mechanism. During the interaction, consumption rate of OH increased at convex corners due to the non unity Lewis number effect. However, the rate of this increase is different for the two kinetics model, with the reaction rate of the Chen 9 species reduced mechanism higher than for the Chen 14 species reduced mechanism throughout the whole flame.

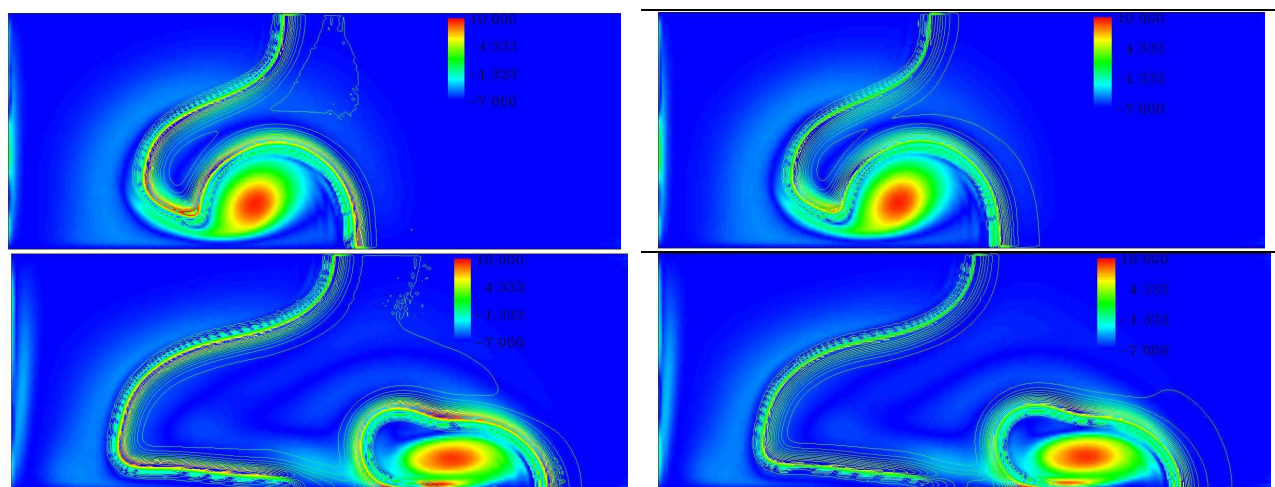


Figure 3.3-1: OH reaction rate contour plot superimposed onto vorticity surface plot for 5 step reduced mechanism at t= a) 0.000512, b) 0.00102 sec and for 10 step reduced mechanism at t= c) 0.000512, d) 0.00102 sec

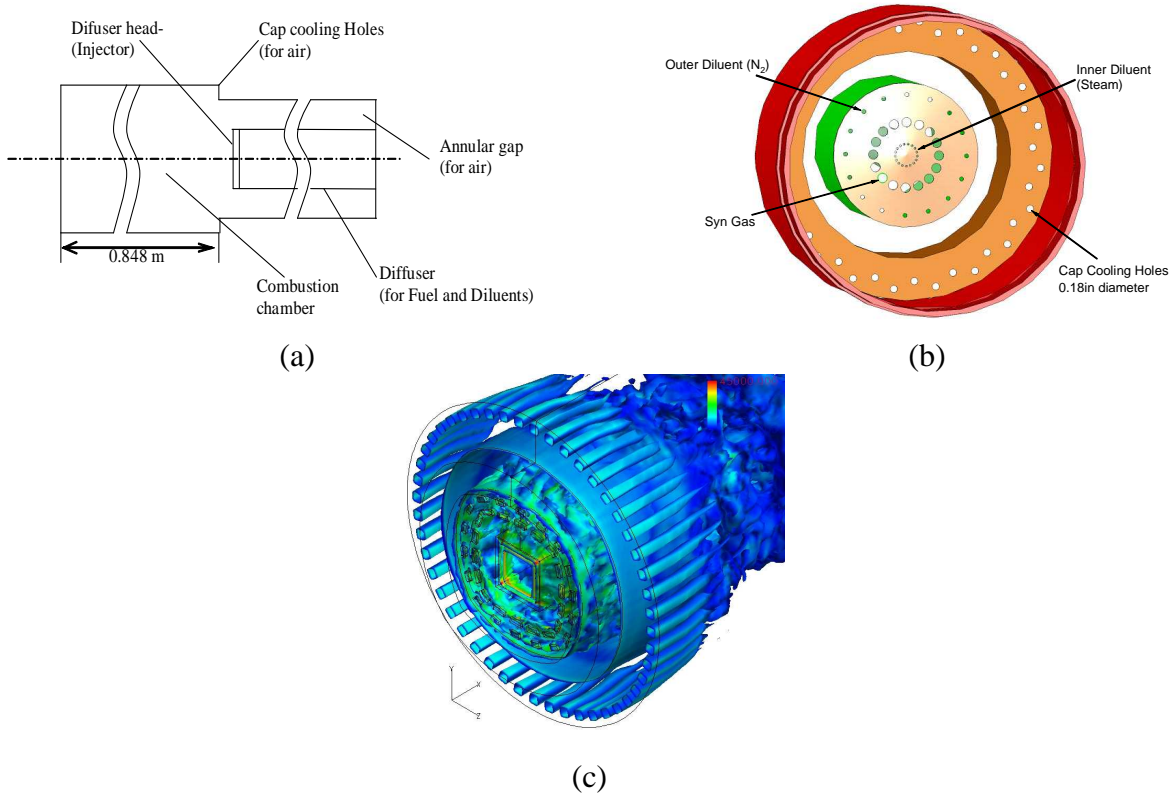


Figure 3.3-2: a) Side view of the schematics of the combustor assembly, b) schematic view of the diffuser cap on the injection plane, and c) perspective view of the grid employed for the computations.

### 3.3.2 LES Computations

LES computations have been performed for a GE combustor geometry with a particular synthesis gas fuel composition. Schematics of the combustor and a close-up view of the flow field are given in Figure 3.3-2. In this combustor configuration, air is injected through an annular gap without any swirl, whereas fuel and diluents (N<sub>2</sub> and H<sub>2</sub>O) are injected by a diffuser cap. The diffuser provides swirl for an outer diluent (N<sub>2</sub>) and fuel. The inner diluent (H<sub>2</sub>O) is injected in such a way as to avoid the diffusion of fuel into the inner section of combustor, so that an effective level of mixing between air and fuel is achieved. Finally, there is another air stream that is used for cooling the walls of the combustion chamber. Except for the main air stream, all other species are injected through set of holes with different diameters and orientations which enhances the mixing.

The LES computations are a continuation of those reported in the previous period. Those results, however, suggested some minor changes were required on the computational grid. Outflow boundary conditions implemented in the code require no reverse flow at the outflow boundary; this constraint was ensured by adding a small convergence section at the end of the computational geometry. The number of grid points on the stream wise direction is increased accordingly. As the flame zone is far upstream, the combustion process is not affected by this addition. Another problem with the previous grid was that the mixing zone between the fuel and diluent streams did not have sufficient resolution to fully resolve the shear layer region. Thus, additional computational nodes are added in-between these two streams to increase the computational stability and accuracy. The final version of the computational grid uses  $210 \times 110 \times 145$  (cylindrical) and  $210 \times 37 \times 37$  (Cartesian), with a total of 3,332,496 grid points, and is shown in Figure 3.3-3.

For LES computations, the location of the cut-off between resolved and unresolved scales is very important and this is dictated by the grid that is employed. The quality of the final version of the grid that is used for our computations is checked by analyzing the spectra of the instantaneous  $u$  and  $v$  velocity time trace data, which is measured at  $x=0.0211$ ,  $y=0.0402$  m. The spectra for both data are given in Figure 3.3-4 along with the  $-5/3$  Kolmogorov scaling of the inertial range. It can be seen that some portion of the inertial range is properly resolved in high turbulence region and therefore, this grid is considered acceptable for the LES.

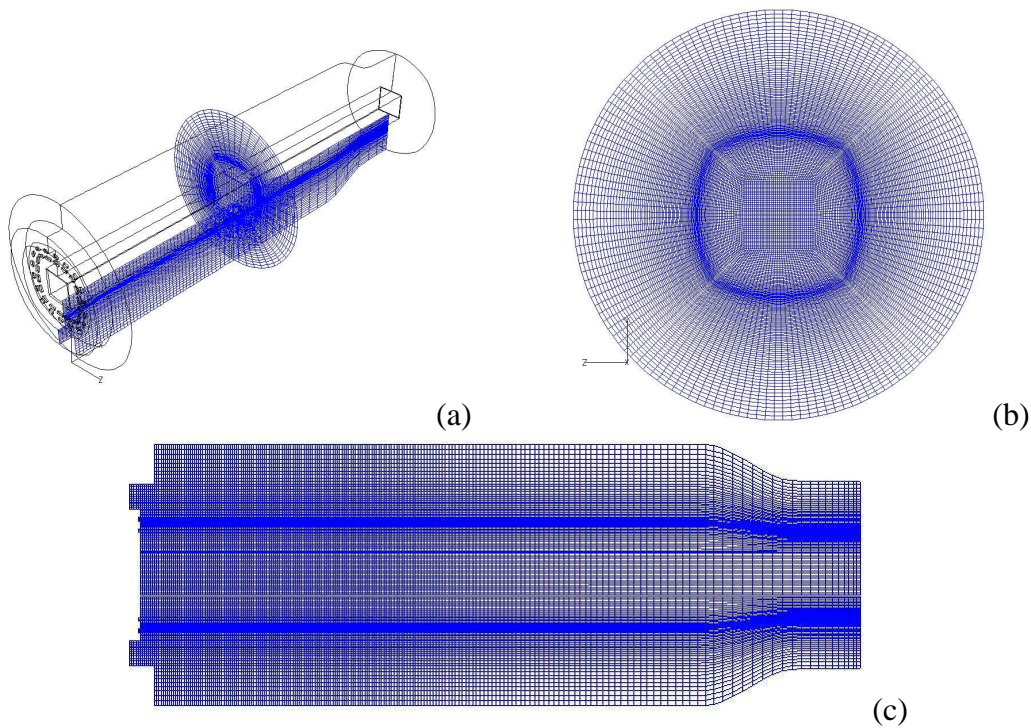


Figure 3.3-3 (a) perspective, (b) cross sectional, and (c) side view of the grid used for computations. Not all grid points are shown.

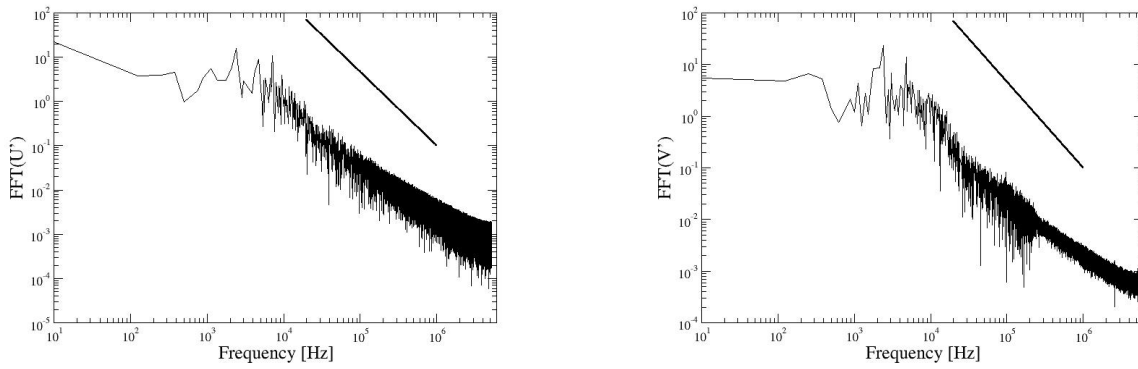


Figure 3.3-4 Spectra obtained from instantaneous U and V velocity data, probed at  $(x,y) = (0.0211, 0.0402)$  m.

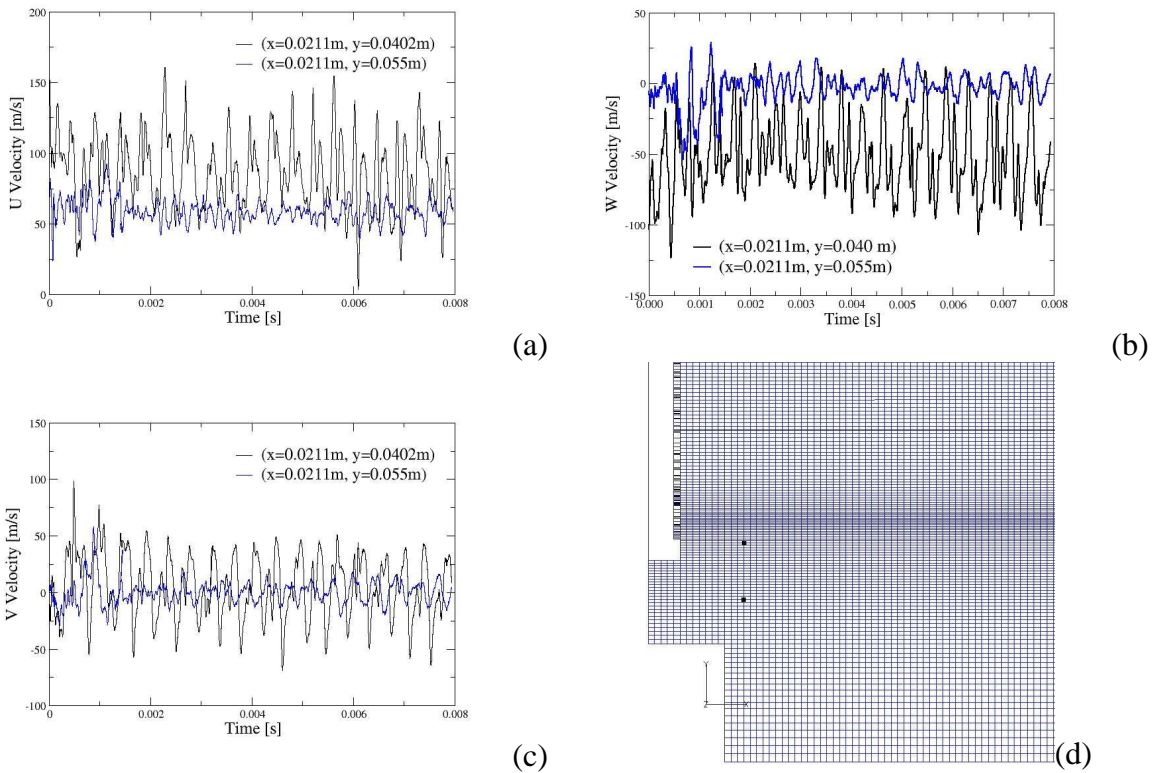


Figure 3.3-5 Time trace of (a) u velocity, (b) w velocity, and (c) v velocity at two different locations; and (d) location of the points where data are from.

Time traces of the velocity components and two different locations,  $(x,y) =$  (a)  $(0.0211, 0.0402)$  and (b)  $(0.0211, 0.055)$  m are given in Figure 3.3-5. Both data are obtained from the same  $x$  and  $z$  locations but different  $y$ . First location is a point which is in-between the diluent and the air stream, whereas the second one is located downstream of the air stream. Hence,  $v$  and  $w$  components of the data obtained from second point fluctuates around approximately a zero mean since the air stream is not swirling. On the other hand, time trace of the  $v$  and  $w$  data obtained from first point shows highly swirling flow at this location. A frequency of around 3 KHz is seen in the time trace and in the movies that appear to correspond to the flapping of the fuel and outer diluent jets, which can be seen in the following figures.

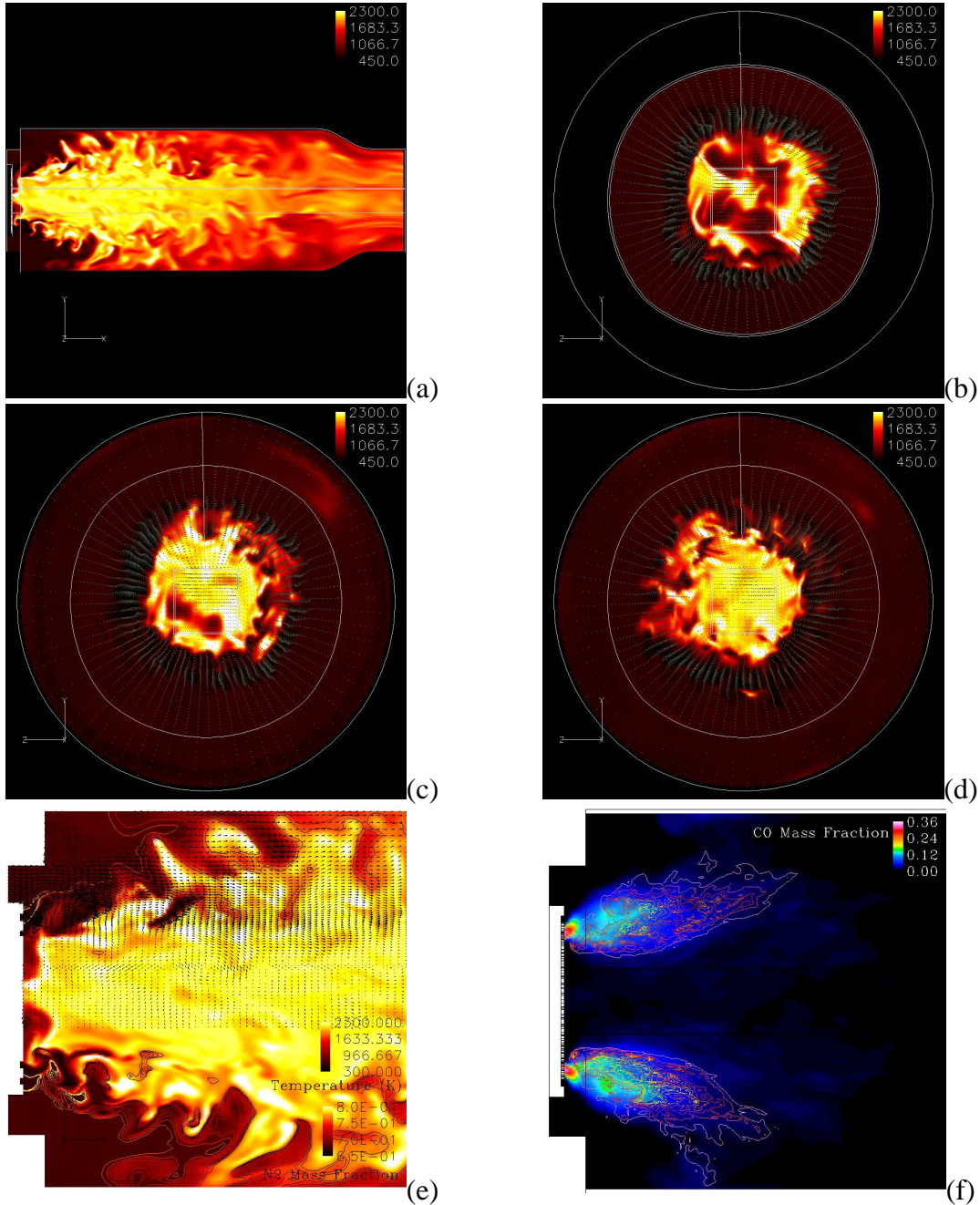


Figure 3.3-6 Instantaneous surface plots of temperature superimposed onto velocity vectors: (a) side view; cross sections obtained at (b)  $x=0.01239$  m, (c)  $0.0182$  m, (d)  $0.0270$  m away from the diffuser cap, and (e) close up side view along with  $N_2$  mass fraction contour

Instantaneous profiles of temperature, velocity vectors,  $N_2$  mass fraction, CO mass fraction and its reaction rate from several different locations are given in Figure 3.3-6. The temperature field shown in Figure 3.3-6(a) suggests that the flame is anchored in the shear layer and then spreads downstream and in the circumferential direction as the effect of the air inlet vanishes, and is eventually convected as far as the walls of the combustor. After this region the downstream temperature is greater than  $1300$  K at all points up to the exit plane. Maximum temperature occurs in the shear layer. The region between the shear layers contains hot gases that are convected upstream due to recirculation zone (Figure 3.3-6e). The recirculation zone acts as a pre-heater for the incoming fuel jet.

The effect of outer diluent,  $N_2$ , is predominant very close to the diffuser cap and acts as a dilution region between fuel and air streams and prevents early ignition. This phenomenon is supported by the time averaged profiles of CO mass fraction and its reaction rate, which is given in Figure 3.3-6(f). Here, reaction rate contour plot surrounds the whole CO stream except for the region close to the outer diluent.

Temperature profiles obtained at three cross sections follows the same physics explained above. Very close to the diffuser cap high temperature region is bounded by the swirling fuel and outer diluent jets, and is a result of the flow recirculation zone that occurs on  $x$ - $y$  plane. As we proceed downstream, a secondary burning zone appears in pockets. Further upstream the secondary flame zone grows bigger and merges with the inner region.

Instantaneous profiles of CO mass fraction and reaction rate are shown in Figure 3.3-7(a) and vorticity contours are presented in Figure 3.3-7(b). Effect of injection from many holes is apparent as the CO mass fraction contours show a discontinuous surface. Side view plot and movies made for the time evolution of CO show the rotating flapping of the fuel and outer diluent jets. Neither side nor the cross sectional views are symmetric along the center  $x$ - $z$  plane.

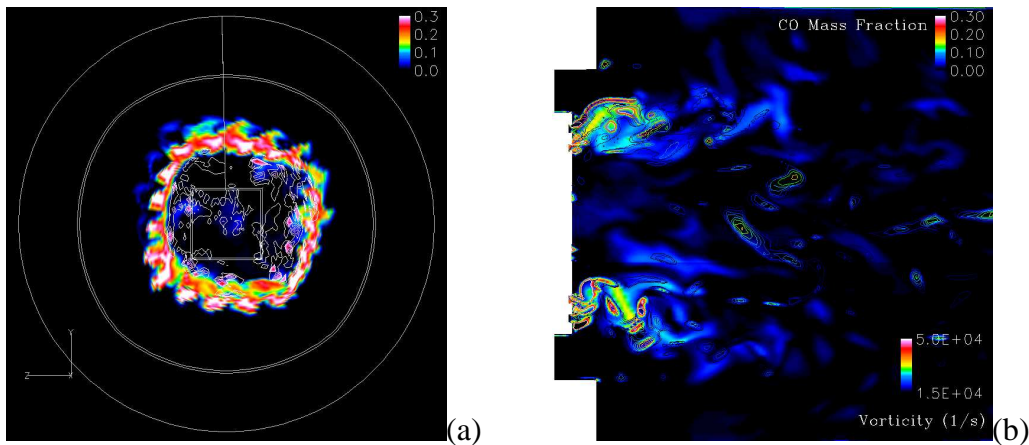


Figure 3.3-7(a) CO mass fraction surface plot with CO reaction rate contour plot obtained at  $x=0.01239$  m away from the diffuser cap. (b) Close up side view of CO mass fraction surface plot with vorticity contour plot.

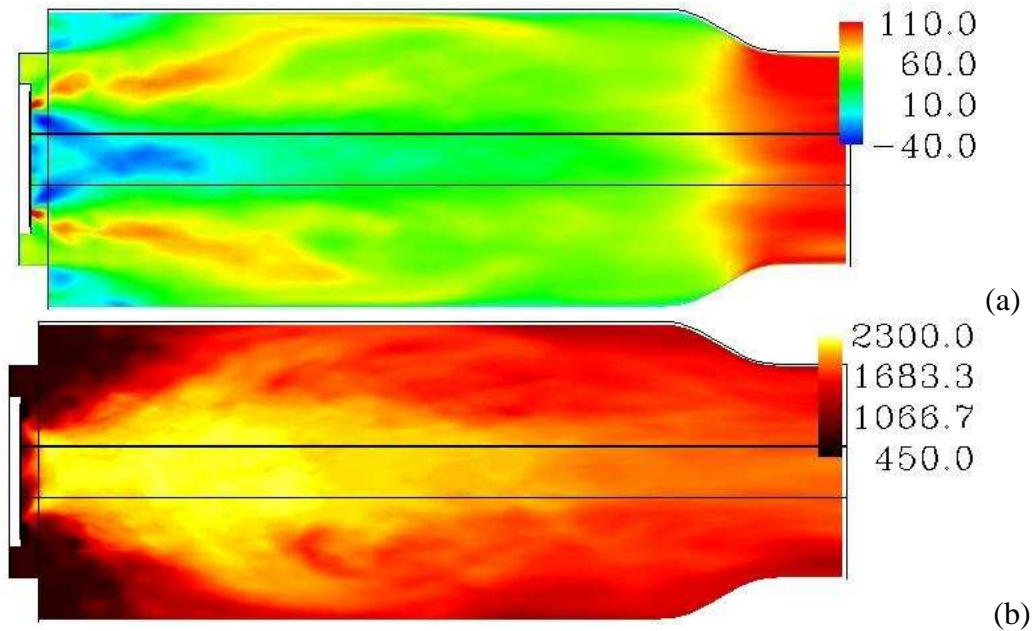


Figure 3.3-8 Time averaged profiles of (a)  $u$  velocity and (b) temperature.

Time averaged surface plots of temperature and  $u$  velocity component are shown in Figure 3.3-8. Two flame “wings” on either side of the center is apparent in this plot as time averaging smoothed the effect of the wrinkling caused by the shear layer. Along the centerline, close to the diffuser cap a low temperature region can be observed which is due to the inner diluent stream ( $H_2O$ ). The velocity of this stream is so low that it can not penetrate further and is squeezed in this region. As the wings hit the walls they are quenched and the center part of the combustor remains the only place with highest temperature.

Recirculation region on the center is viewed better by the time averaged  $u$  velocity profiles given in Figure 3.3-8(b). Injection of inner diluent decreases the strength of this zone early upstream on the center but the reversed flow caused by swirling fuel and outer diluent jets felt very strong close to their corresponding injection planes on either side of the center line and they tend to merge on the upstream direction. There is another recirculation zone formed by the dump plane on upper and lowermost regions of the plot. The cooling air stream emerging onto this region is not very powerful to affect the size of the region, and it vanishes as soon it is injected.

## 4 Conclusions

### 4.1 Task 3 (Syngas fuel flame characterization)

The effect of preheating and CO<sub>2</sub> dilution have been studied using a burner stabilized, stagnation flame configuration for a 50:50 H<sub>2</sub>:CO fuel mixture for which larger discrepancies have been observed between the previous Bunsen flame measurements and simulation results. Results indicate that at 600 K preheat temperature and 0.8 equivalence ratio, all the model predictions are in good agreement with measurements. As the preheat temperature increases to 700 K and  $\phi$  is decreased to 0.6 (more lean mixtures), the discrepancies increase to as much as 20% for the predictions with the detailed Davis and reduced Chen 9 species mechanisms. Dilution of the fuel with even 40% CO<sub>2</sub> does not change the degree of agreement between the models and experiments. This indicates that the spectral radiation reabsorption of CO<sub>2</sub> dilution is not a major issue for these mixtures. For all the cases studied, the 14 species Chen mechanism predictions at high temperature have the best agreement with the measurements. Similarly, the discrepancy between the measurements and the Chen 9 species mechanism predictions are always the greatest. Therefore, the experiments suggest that the reduced 14 species mechanism by Chen is the superior choice for the high temperature reactant gas conditions expected in the gas turbine environment. In addition with 10% or better agreement with the experiments, the mechanism should not require changes to make reasonably accurate predictions in the LES modeling.

### 4.2 Task 5 (Prototype Design)

A prototype TVC combustor was designed, manufactured, and operated on syngas fuel at high pressure and air preheat temperatures. The syngas was representative of an EECF fuel. The combustor operated with very low combustion dynamics, 0.5 psi p-p. The combustor surface temperatures fell within acceptable limits for the prototype. High preheat temperatures representative of gas turbine compressor discharge temperatures were used. The premixers mixed the hydrogen containing syngas (24%) with air without flashback of the flame into the premixer. Emissions from the combustor demonstrated low NO<sub>x</sub> levels below 5 ppm after correction for 15% O<sub>2</sub>.

The TVC syngas combustor has met a significant milestone demonstrating premixed syngas operation without flashback. The combustor also performed in a manner consistent with premixed performance, namely low NO<sub>x</sub> emission. Further evaluations will now be performed exploring the performance over the targeted fuel space.

### 4.3 Task 6 (Syngas Methodology for Advanced CFD Tools)

A reduced 5-step 9 species chemical kinetic mechanism for syngas combustion has been developed. The physics of the mechanism have been established through validation with the experimental data obtained in Task 3. The reduced mechanism predicts flame behavior relatively well over a wide range of fuel compositions and equivalence ratios. However, the

mechanism has not been fully validated against high-pressure data and fails to accurately predict the influence of pre-heating. Future plans include comparing predictions using the reduced mechanism with more high-pressure data and investigating the discrepancy with pre-heat. The accuracy of the reduced kinetic mechanism to predict detailed flame structure has been investigated by comparison of results obtained from detailed kinetic mechanisms for simplified reactor models and DNS simulations of flame vortex interaction. The reduced kinetic mechanism gives results similar to those obtained with the more detailed kinetic mechanisms. The velocity profiles and estimated flame structure are nearly identical for both the reduced and detailed mechanisms. The advantage of the reduced mechanisms is in computational costs, which is desirable for LES of full-scale combustors.

Large eddy simulations (LES) were performed for the hybrid nozzle prototype combustor geometry under conditions similar to an industrial gas turbine. The LES solves for the flow structures at a scale larger than the grid size. The sub-grid convection, diffusion and chemical reactions of species are calculated using a one-dimensional linear eddy model (LEM). Calculations are performed for an overall lean swirling syngas/air flame using the reduced kinetic mechanisms. Vortex breakdown and hot products recirculation are predicted. The flame is predicted stable and forms in the shear layer between the air/outer/diluent/syngas passage. The cap cooling air minimizes heat transfer at the combustor dump plane and helps establish recirculation of the hot products. As per the design requirement, the inner diluent jet helps with flame lift-off and to keep the diffusion tip cool. Future work will implement the LES with the reduced chemical mechanism developed for syngas and using sub-grid methods for 3D analysis and comparison with experimental data that will be obtained as part of Task 5.

## 5 References

Andrews, G. E., and Bradley, D. (1972). "Determination of burning velocities – Critical review." Combustion and Flame **18**: 133-153.

Davis, S.G., Joshi, A.V., Wang, H., and Egolfopoulos, F.N, *Proc. Comb. Inst.* **30**: 1283-1292 (2004).

- Egolfopoulos, F. N., Cho, P., and Law, C. K. (1989). "Laminar flame speeds of Methane-Air mixtures under reduced and elevated pressures," *Combustion and Flame* **76**: 375-391.
- Egolfopoulos, F. N., Zhang, H., and Zhang, Z. (1997). "Wall effects on propagation and extinction of steady, strained, laminar premixed flames," *Combustion and Flame* **109**: 237-252.
- Iyer, V. A., Haynes, J., Anand, A., and May, P. (2005). "Evaluation of Emissions Performance of Existing Combustion Technologies for Syngas Combustion," Proceedings of *ASME Turbo Expo* 2005, GT2005-68513, June 6-9, 2005, Reno-Tahoe, Nevada, USA.
- Kempf, A., Lindstedt, R.P., Janicka, J., "Large-Eddy Simulation of a Bluff Body Stabilized Nonpremixed Flame", *Combustion and Flame*, Article in press.
- Kim, W.-W., Menon, S., and Mongia, H. C., "Large-Eddy Simulation of a Gas Turbine Combustor Flow" *Combustion Science and Technology*, Vol. 143, 1999, pp. 25-62.
- Maas, U., and Pope, S.B., "Simplifying Chemical Kinetics: Intrinsic Low-Dimensional Manifolds in Composition Space" *Combustion and Flame*, Vol. 88, 1992, pp.239-264.
- Mahesh, K., Constantinescu, G. and Moin, P., "Large-Eddy Simulations of Gas Turbine Combustors", *Center for Turbulence Research Annual Research Briefs*, 2000.
- McLean, I. C., Smith, D. B., and Taylor, S. C. (1994). "The use of carbon monoxide/hydrogen burning velocities to examine the rate of the CO + OH reaction." *Proceedings of the Combustion Institute* **25**: 749-757.
- Meier, W., Duan, X.R., Weigand, P., "Investigations of Swirl Flames in a Gas Turbine Model Combustor II. Turbulence-Chemistry Interactions", *Combustion and Flame*, Article in press.
- Menon, S. and Calhoun, W., "Sub-grid Mixing and Molecular Transport Modeling for Large-Eddy Simulations of Turbulent Reacting Flows" *Proceedings of the Combustion Institute*, Vol. 26, 1996, pp. 59-66.
- Meyer, T.R., Roy, S., Lucht, R.P. and Gord, J.R., "Dual-Pump Dual-Broadband CARS for Exhaust-Gas Temperature and CO<sub>2</sub>-O<sub>2</sub>-N<sub>2</sub> Mole-Fraction Measurements in Model Gas-Turbine Combustor", *Combustion and Flame*, Vol. 142, 2005, pp. 52-61.
- Mueller, M.A., Yetter, R.A., and Dryer, F.L., *International Journal of Chemical Kinetics* **31**: 705-724 (1999).
- Pitsch, H., "A Consistent Level Set Formulation for Large Eddy Simulation of Premixed Turbulence", *Combustion and Flame*, Vol. 143, 2005, pp. 587-598.
- Pope, S.B., "Computationally Efficient Implementation of Combustion Chemistry Using in situ Adaptive Tabulation" *Combustion Theory and Modelling*, Vol. 1, 1997, pp. 41-63.

Pope, S.B., Turbulent Flows. Cambridge University Press, 2000.

Sankaran, V. and Menon, S., “Sub-grid Combustion Modeling of 3-D Premixed Flames in the Thin-Reaction-Zone Regime,” *Proceedings of the Combustion Institute*, Vol. 30, 2004.

Weigand, P., Meier, W., Duan, X.R., Stricker, W., Aigner, M., “Investigations of Swirl Flames in a Gas Turbine Model Combustor II. Flow Field, Structures, Temperature and Species Distributions”, *Combustion and Flame*, Article in press

Zhu, D. L., Egolfopoulos, F. N., and Law, C. K. (1988). “Experimental and numerical determination of laminar flame speeds of methane/(Ar, N<sub>2</sub>, CO<sub>2</sub>) – air mixtures as function of stoichiometry, pressure, and flame temperature.” Proceedings of the Combustion Institute **22**: 1537-1545.